学位論文（要約）

Northwestern Australian sea level records during Marine Isotope Stage 2 from marine sediment cores and glacial isostatic adjustment model

（海洋堆積物コアと GIA モデルによる北西オーストラリアにおける
海洋酸素同位体ステージ 2 の相対的海水準の復元）

平成 28 年 12 月博士（理学）申請

東京大学大学院理学系研究科
地球惑星科学専攻

石輪　健樹

Northwestern Australian sea level records during Marine Isotope Stage 2 from marine sediment cores and glacial isostatic adjustment model

Takeshige Ishiwa

Department of Earth and Planetary Science, and

Atmosphere and Ocean Research Institute,

The University of Tokyo

submitted to The University of Tokyo

in partial fulfillment of the requirements for Degree of Doctor of Philosophy

December 2016

This dissertation is dedicated to my late father

Acknowledgements

My sincere gratitude goes first to Dr. Yusuke Yokoyama, being my advisor and encouraging me to proceed with this research. Completion of this thesis would not be impossible under the direction of Dr. Yusuke Yokoyama. He has given me great opportunities to recognize what the international and competent researcher is. My mother and sister provided a plenty of supports and patience to me during the Ph.D. course. Without their supports, I could not accomplish this thesis to the end. I appreciate Dr. Stephen Obrochta for giving me significant advices and taking a lot of time to improve my English. Dr. Yosuke Miyairi gave me the first step to do geochemical experiments and useful advice to proceed with my research correctly. Dr. Minoru Ikehara provided me valuable place and time at the Center for Advanced Marine Core Research, Kochi University, and gave me helpful advice especially to the experiments of geochemical and major elemental analyses. Dr. Jun'ichi Okuno taught me how to use glacial isostatic adjustment model and helped me for interpreting the results of this thesis. Dr. Katsuto Uehara provided the tidal model and taught me how to use it. He also gave me the opportunity to discuss the results. Dr. Takenori Sasaki provided the opportunity to detect the molluscan species. Dr. Akihisa Kitamura gave me useful advice to my study. Dr. Wataru Sakashita gave me a plenty of comments to improve this study. Dr. Masako Yamane checked the manuscript and gave ma a plenty of advice. Ms. Tomoko Bell also checked this manuscript and improved my English. The member of Yokoyama's Laboratory and OFGS gave me a lot of advice to proceed with this research and shared significant time to encourage my research life at the Atmosphere and Ocean Research Institute. I thank the member of KH11-1 cruise for operating the cruise and collecting the samples and data. A part of my study was supported by the grant of the Japan Society for the Promotion of Science Fellows DC2 and the cooperative research program of the Center for Advanced Marine Core Research. I appreciate a lot of mentors, colleagues, and friends for giving a plenty of advice and opportunities to complete my thesis.

Abstract

Global sea level change in the glacial-interglacial cycles has been fluctuated with global ice volume change and also closely related to global and regional climate variabilities. A further understanding of climate variabilities requires the information of the timing and amplitude of sea-level change. Marine Isotope Stage 2 (MIS 2) is the latest glacial period (30,000–15,000 years ago), including the Last Glacial Maximum (LGM) characterized by the maximum of global ice volume. There are a plenty of paleoclimatic records during MIS 2 because this period is within the applicable age of radiocarbon dating, which is the widely accepted measurement. The comparison of various paleoclimatic records with sea-level change derives an understanding of the earth climate system. However, global sea-level change during MIS 2, especially the LGM, is less understood due to its paucity of data and its uncertainty. The Bonaparte Gulf, northwestern Australia, is a suitable region to reconstruct the global sea level change since the Gulf is far from the former ice sheet and tectonically stable. Marine sediment cores in the Bonaparte Gulf therefore could provide the accurate sea-level records during MIS 2.

The main objective of this thesis is to reconstruct sea-level change during MIS 2 and revise the global ice volume history during the LGM. To achieve this objective, I constructed this thesis structure as follows. First, the sedimentary environment in the Bonaparte Gulf is discussed to evaluate the response to sea-level change during MIS 2 (*Chapter 2*). Second, exceeding 250 radiocarbon dates of sediment cores with various and continuous depths provide relative sea-level change in the Bonaparte Gulf (*Chapter 3*). Third, the new ice volume equivalent sea level (ESL) is proposed based on relative sea-level change discussed in *Chapter 3* using the glacial isostatic adjustment (GIA) model (*Chapter 4*). Finally, the comparison of the new ESL curve with other global sea level records and the implication for the relation with climate change are discussed (*Chapter 5*).

Sedimentary environmental change in the Bonaparte Gulf during Marine Isotope Stage 2 (Chapter 2): The Bonaparte Gulf, located in the northwestern Australian continental shelf, is the widest in the world with shallow carbonate terraces and platforms that were exposed during lower sea level. The dominant sediments type switches between carbonate and siliciclastic over a sea-level cycle. However, the mechanism of sedimentary environmental change in the Bonaparte Gulf is not well understood. The Bonaparte Gulf is known as one of the gulf influenced by large tide, up to 6.0 m, corresponding to the volume of Greenland Ice Sheet. Researches on past tidal range are required to reconstruct an accurate sea-level change. I present a record of sedimentary environmental change from ca. 35 to 24 cal kyr BP (calendar age kilo years before present), which is related to a sea-level variability and exposure of carbonate terraces and platforms. Multi-proxy data from a marine sediment core shows a sea-level change induced change in sedimentary environment from siliciclastic to carbonate-dominated sedimentation during the last glacial. Radiocarbon ages show the timing of this switch occurred at ca. 26 cal kyr BP, associated with a local sea-level fall from -60 to -90 m. Tidal range during the lower sea level was negligible for sedimentary environmental change due to the protection of carbonate terraces and platforms from wave activity of the Timor Sea.

Marine Isotope Stage 2 relative sea-level records from sediment cores in the Bonaparte Gulf (Chapter 3): Yokoyama et al. [2000] reported that the LGM was terminated abruptly at ca. 19 cal kyr BP with a rapid sea-level rise (19 ka event) using marine sediment cores from the Bonaparte Gulf. Their sea-level reconstruction defined the age of the LGM termination, but the timing of its initiation was less constrained, partly because the number of radiocarbon analyses was limited to clarify the LGM duration. Here I document the MIS 2 sea level records using marine sediment cores with various depths from the Bonaparte Gulf, which would provide high-resolution information of paleo-water depth at the time of deposition. Sedimentary environments were determined using benthic foraminifera and geochemical analysis. More than 250 radiocarbon dates on carbonates and bulk organic matters provide precise age-depth models. The results reveal that relative sea level shows the short LGM duration of ca. 1,000 years at ca. 19 cal kyr BP. The pre-LGM sea level located a ca. 5 m shallower position than previous works suggested.

Ice volume equivalent sea level based on relative sea-level records from the Bonaparte Gulf using glacial isostatic adjustment model (Chapter 4): Global ice volume change is obtained using the glacial isostatic adjustment (GIA) model. However, ice volume history in GIA model (ESL: ice volume equivalent sea level) during the LGM is less constrained due to the paucity of observations. I propose a new ESL model based on results from GIA model and new relative sea-level records for the Bonaparte Gulf. This model could explain well with other MIS 2 sea-level records.

Contents

本章は，5 年以内に雑誌等で刊行予定のため非公開.

本章は，5 年以内に雑誌等で刊行予定のため非公開.

本章は，5 年以内に雑誌等で刊行予定のため非公開である第 3 章・第 4 章を含むため，一部非公開.

Chapter 1 General introduction

1.1 Climate variability during Marine Isotope Stage 2

Quaternary sea-level has fluctuated associated with continental ice volume change (Figure 1.1-1), which is related to abrupt climate changes recorded in high-latitude ice cores and marine sediment cores [Dansgaard et al., 1989; Bond et al., 1992; Lambeck et al., 2002a; Naafs et al, 2013a]. Freshwater discharge to the ocean has influenced ocean circulations [Heinrich, 1988; Bohm et al., 2015; Hemming, 2004; Otto-Bliesner and Brady, 2010]. The shape of ice sheets also has an impact on atmospheric circulation [Manabe and Broccoli, 1985; Oka et al., 2012; Vettoretti and Peltier, 2013; Zhang et al., 2014], leading to sea ice extension (Figure 1.1-2). The response of atmospheric and ocean circulations to climate change also changes associated with the rate of exposure of continental shelf, which is fluctuated with a sea-level change (Figure 1.1-3) [Chivas et al., 2001; DiNezio et al., 2011, 2016; DiNezio and Tierney, 2013]. A further understanding of sea-level change as the indicator of global ice volume is required to elucidate global and regional climate variability in the glacial period.

Marine Isotope Stage 2 (MIS 2) is known as the period of expansion of continental ice sheet in a high-latitude region [Lambeck and Chappell, 2001; Yokoyama and Esat, 2011]. This period contains the Last Glacial Maximum (LGM), characterized by the maximum volume of the global ice sheet (Figure 1.1-1). Global sea level fell to approximately -130 m during the LGM because ice sheets had been developed in high-latitude continents and mountain glaciers (Figure 1.1-4) [Fleming et al., 1998; Yokoyama et al., 2000a, 2001a; Clark and Mix, 2002; Clark et al., 2009]. This period was within the applicable age of radiocarbon dating, providing a sea-level comparison with other paleoclimatic records [Lambeck et al., 2014; Yokoyama and Esat, 2011]. This comparison provides a useful test of climate model to improve its accuracy for the prediction of future climate change [Mix et al., 2001].

The mechanism of growth of ice sheet has been suggested to describe global sea level fall to its minimum [Cutler et al., 2003; Clark et al., 2009; Abe-Ouchi et al., 2013]. Snow accumulation drives positive feedbacks of ice sheet growth since its high albedo causes regional temperature lowering, reduces melting on the surface and enhances snow accumulation [Ruddiman et al., 1980; Cutler et al., 2003]. Summer insolation of 60ºN decreased during MIS 2 and had reached its minimum at 25 cal kyr BP (calendar kilo years before present), and this caused the growth of ice sheet [Clark et al., 2009; Cutler et al., 2003].

The onset of deglaciation at ca. 19 cal kyr BP is inferred from the decay of continental ice sheets, which has been recorded in marine sediment cores and corals [Yokoyama et al., 2000a, 2001a; Clark et al., 2004; Peltier and Fairbanks, 2006; Hanebuth et al., 2009]. This timing is almost consistent with increasing summer insolation at northern hemisphere [Clark et al., 2009]. A rapid sea-level rise at the onset of deglaciation was observed in marine sediment cores from the Bonaparte Gulf, northwestern Australia [Yokoyama et al., 2000a, 2001a], being consistent with records in the Sunda Shelf [Hanebuth et al., 2009] and Irish Sea Basin [Clark et al., 2004].

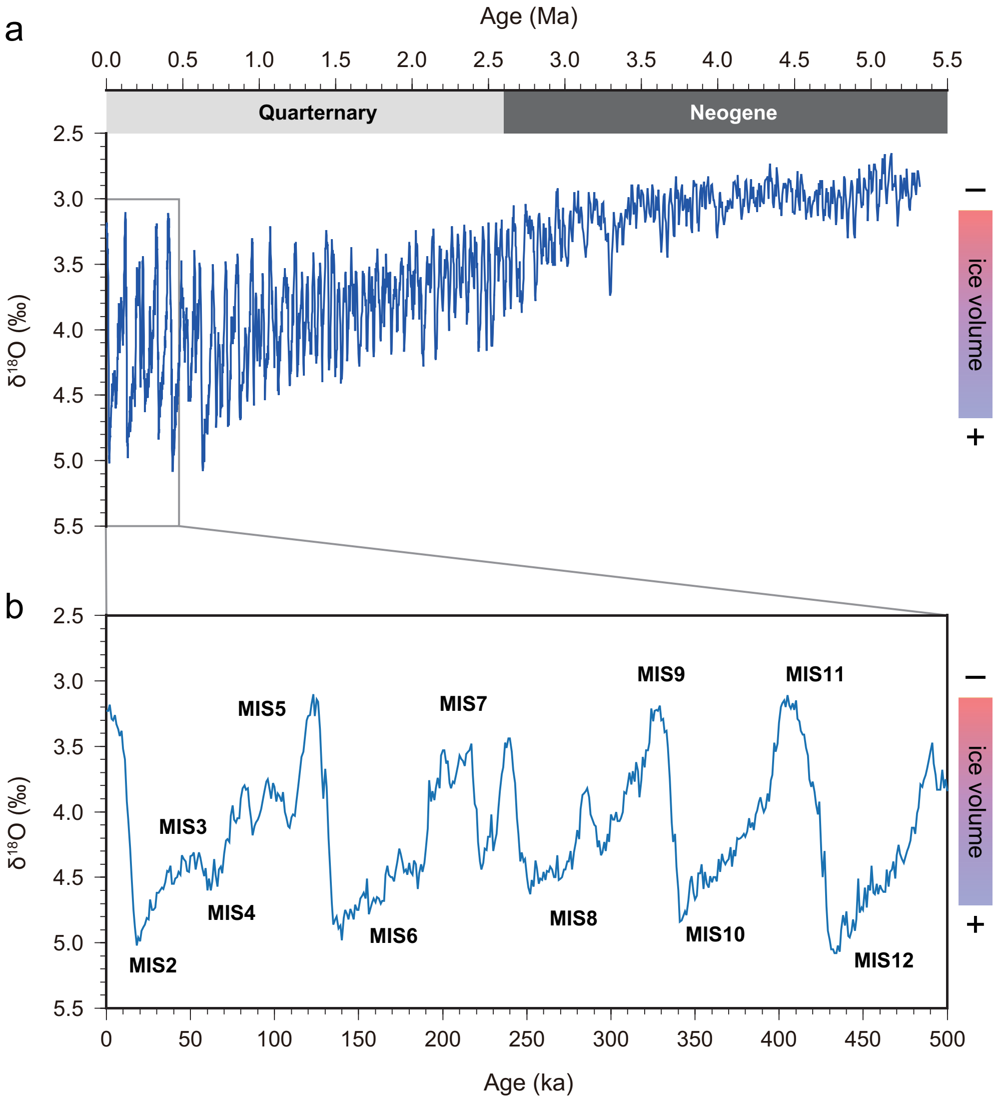

Figure 1.1-1: Variation of benthic oxygen isotope ($\delta^{18}O$) in two time-windows. (a) $\delta^{18}O$ record from LR04 stack curve during 5.5 million years (Ma) [Lisiecki and Raymo, 2005]. (b) $\delta^{18}O$ record during 500-kilo years (ka). Marine Isotope Stage (MIS) are given.

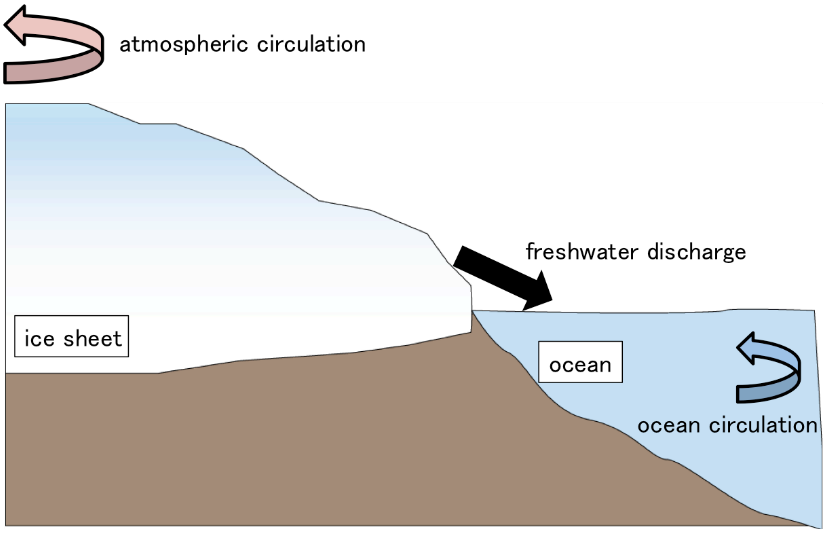

Figure 1.1-2: Schematic illustration of the impact on climate change in ice sheet fluctuations. Freshwater discharge is affected to ocean circulations and shape of ice sheet changes atmospheric circulations.

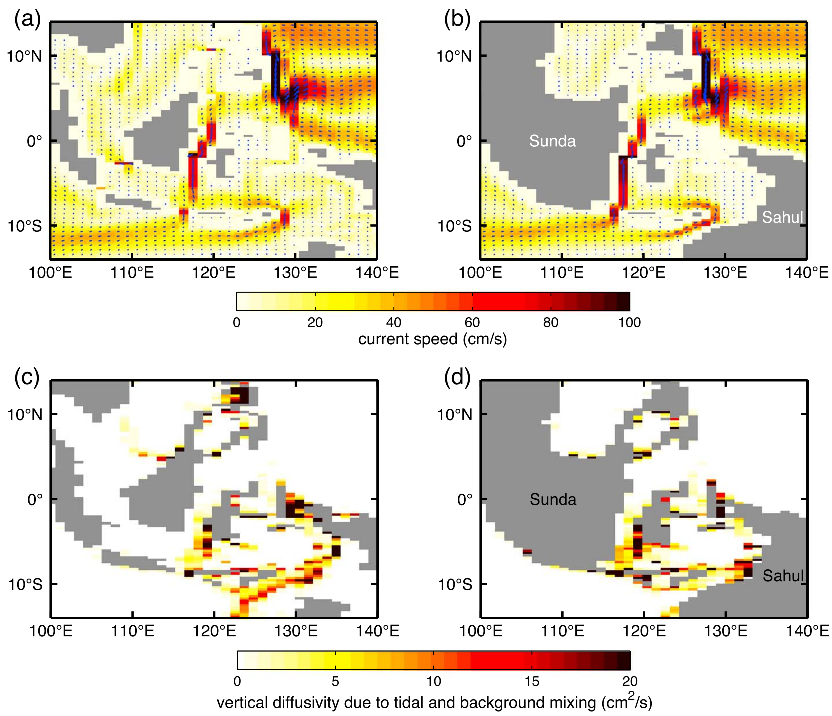

Figure 1.1-3: Simulated ocean circulation change of sea level highstands and lowstands [DiNezio et al., 2016]. (a) present and (b) LGM simulated results. Velocity vectors are averages in upper 50 m. (c) present and (d) LGM vertical differences due to tidal and background mixing at a depth of 100 m.

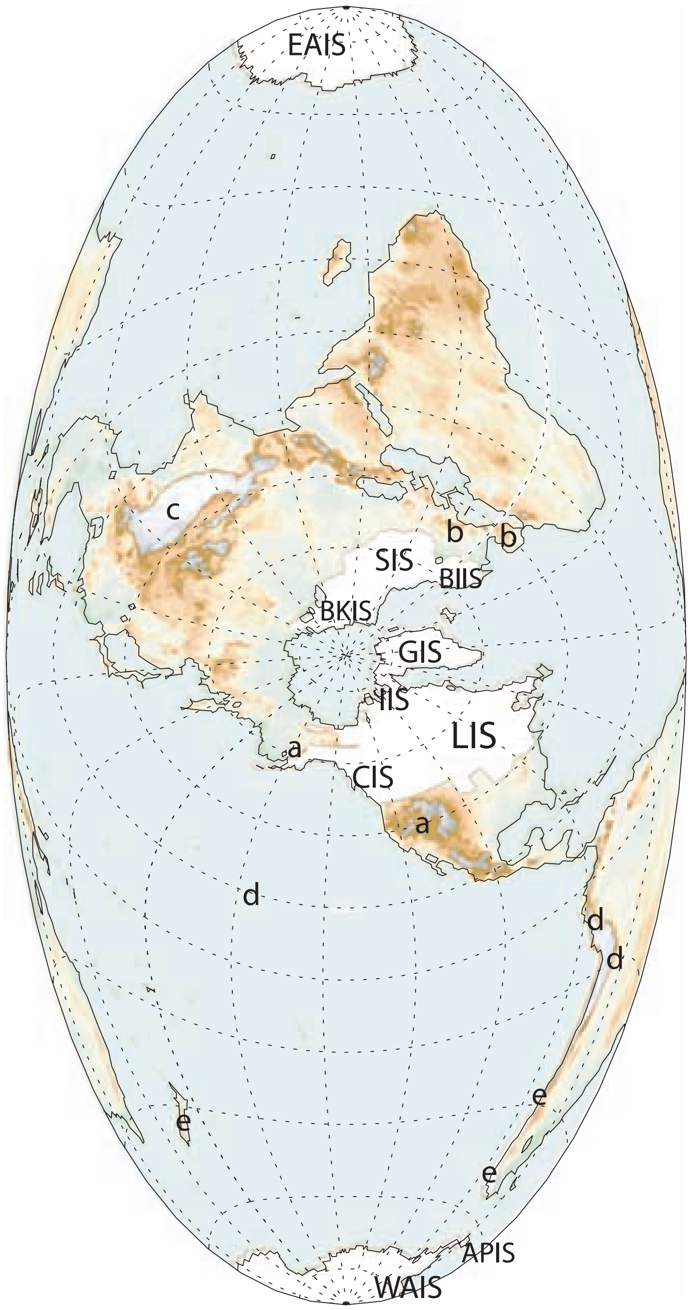

Figure 1.1-4: Distribution of ice sheet during the LGM [Clark et al., 2009]. LIS: Laurentide Ice Sheet, CIS: Cordilleran Ice Sheet, IIS: Innuitian Ice Sheet, BKIS: Barents-Kara Ice Sheet, BIIS: British-Irish Ice Sheet, SIS: Scandinavian Ice Sheet, GIS: Greenland Ice Sheet, WAIS: West Antarctic Ice Sheet, EAIS: East Antarctic Ice Sheet.

1.2 Sea level change during Marine Isotope Stage 2

Global sea-level change has been reconstructed using oxygen isotope ($\delta^{18}O$) records of benthic foraminifera [Shackleton, 1967, 1987; Chappell and Shackleton, 1986; Waelbroeck et al., 2002] and planktonic foraminifera [Siddall et al., 2003; Grant et al., 2012, 2014]. Tracing past shorelines provides sea-level information using corals [Bard et al., 1996; Esat et al., 1999; Cutler et al., 2003; Deschamps et al., 2012; Fairbanks, 1989; Peltier and Fairbanks, 2006; Yokoyama et al., 2001b] and marine sediment cores [Hanebuth et al., 2000, 2009; Yokoyama et al., 2000a, 2001a]. In this section, previous works of MIS 2 sea-level records will be presented.

1.2.1 Oxygen isotope records in marine sediments

Oxygen isotope ($\delta^{18}O$) records of benthic foraminifera are an indicator of global sea level change since the amount effect of evaporation and condensation reflects the global ice volume change (Figure 1.2-1). ^{16}O-rich water evaporates in the ocean and is transported to the high latitude, fixing as ice sheet. As a result, ^{18}O-rich water dominates in the ocean. This mechanism can be observed on $\delta^{18}O$ of benthic foraminifera, which varies in glacial-interglacial cycle [Emiliani, 1955]. After Emiliani [1955], a plenty of works have extended the studies of $\delta^{18}O$ records and discussed the glacial-interglacial climate variability [Shackelton, 1967, 1987; Chappell and Shackleton, 1986; Waelbroek et al., 2002; Cutler et al., 2003; Lisiecki and Raymo, 2005]. Lisiecki and Raymo [2005] compiled 57 benthic $\delta^{18}O$ records and presented 5.3 million years stacked $\delta^{18}O$ curve (LR04) (Figure 1.1-1). However, ice volume records using benthic $\delta^{18}O$ contain uncertainties from regional variability in $\delta^{18}O$ and temperature of sea water [cf., Adkins et al., 2002; Waelbroeck et al., 2002; Cutler et al., 2003].

The Red Sea is sensitive to sea-level change due to the narrow (~20 km) strait and shallow (~130 m) sill [Siddall et al., 2003]. $\delta^{18}O$ values in planktonic foraminifera from the Red Sea sediments provide a centennial-scale resolution sea-level change

(Figure 1.2-2) [Siddall et al., 2003; Grant et al., 2012, 2014; Rohling et al., 2014] since the changes in the profile of strait with a sea-level change influence the exchange of water masses transport though the strait. This sea-level record provides an understanding of global climate since high-resolved and continuous sea-level change can be compared with other climate records (eg., high latitude ice cores and $\delta^{18}O$ values in deep sea sediments) [Rohling et al., 2014]. However, there is no record during the LGM because of the aplanktonic condition, which is high salinity in exceeding 45 psu (practical salinity unit) [Fenton et al., 2000; Siddall et al., 2003]. During this interval, they interpolated the LGM sea level by $\delta^{18}O$ values in benthic foraminifera from Hemleben et al. [1996].

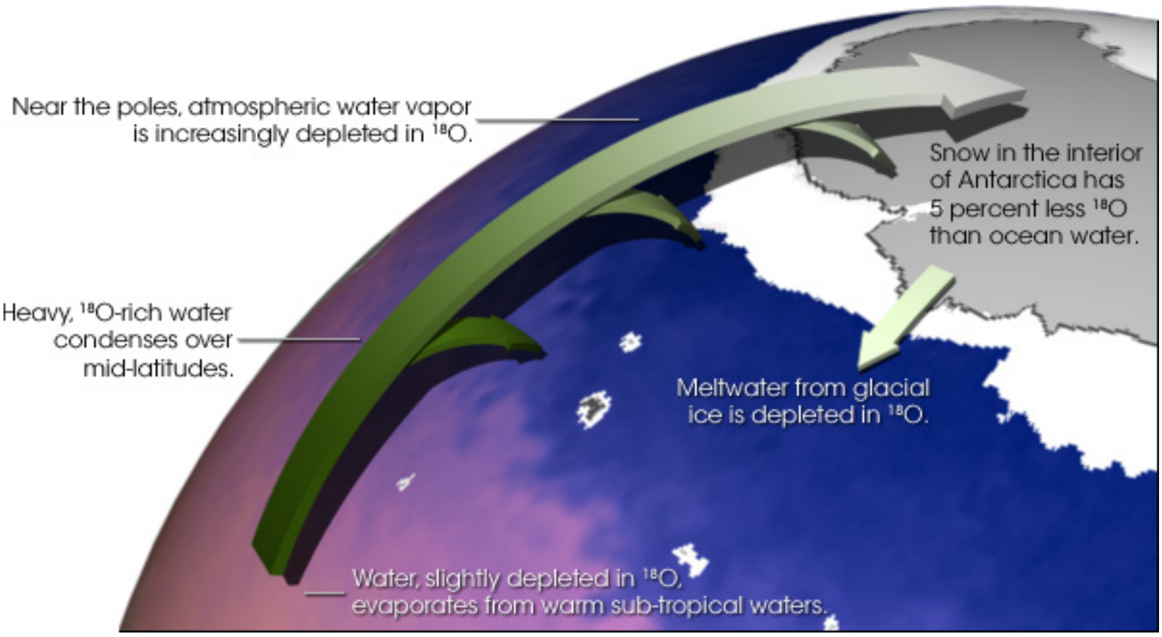

Figure 1.2-1: Schematic illustration of $\delta^{18}O$ variation between ocean and continental ice sheets. [http://earthobservatory.nasa.gov/Features/Paleoclimatology_OxygenBalance/]

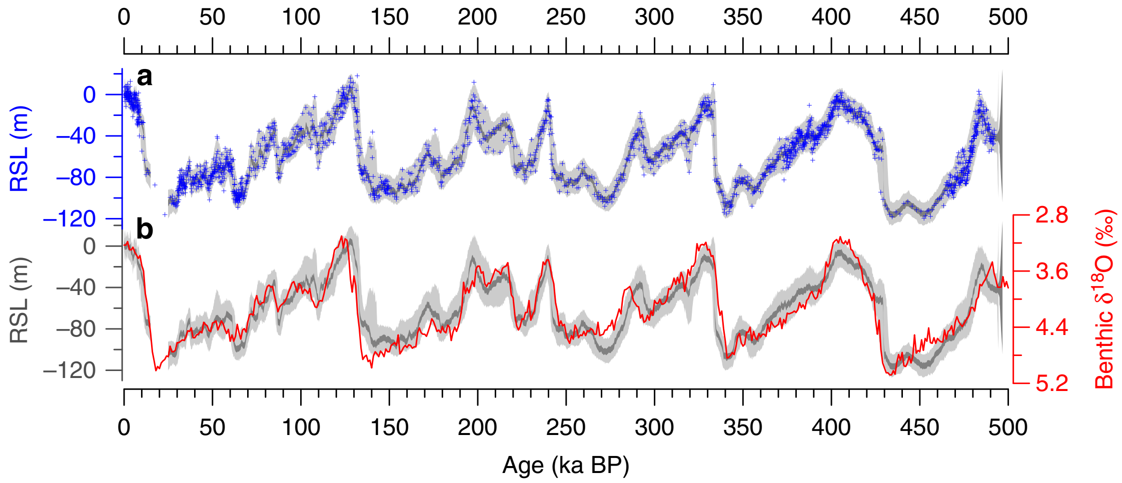

Figure 1.2-2: Red Sea relative sea level record [Grant et al., 2014]. (a) Grey shade corresponds to the 95% probability interval of relative sea level (light grey) and its maximum probability (dark grey). The Red Sea relative sea level dataset is Grant et al. [2012, 2014] (blue dots). (b) Probabilistic relative sea level with superimposed benthic $\delta^{18}O$ records (red line).

1.2.2 Relative sea-level change

Tracing the past shoreline using indicators of shallow sedimentary environments can provide the information of past sea-level change. Observed sea-level change at a site is called as “relative sea level”, calculated as follows:

$$\Delta\zeta_{rsl} = \Delta\zeta_{esl} + \delta\zeta_{water}^{iso} + \delta\zeta_{ice}^{iso} + \delta\zeta_{tect}$$

----------(Eq. 1.2-1)

where $\Delta\zeta_{rsl}$ is the relative sea level and $\Delta\zeta_{esl}$ is the ice volume equivalent sea level (ESL), reflecting global ice volume change history. $\delta\zeta_{water}^{iso}$ and $\delta\zeta_{ice}^{iso}$ are the isostatic effects of sea water and ice sheet, respectively, and $\delta\zeta_{tect}$ is a regional effect, corrected factor of uplift and subsidence. $\delta\zeta_{water}^{iso}$ and $\delta\zeta_{ice}^{iso}$ are calculated by glacial isostatic adjustment (GIA) model [cf., Farrell and Clark, 1976; Lambeck and Nakada, 1992; Peltier and Fairbanks, 2006; Lambeck et al., 2000, 2014].

A relative sea level is an observed sea level at a site, reconstructed by tracing past shorelines using fossil corals [cf., Bard et al., 1996; Cutler et al., 2003; Deschamps et al., 2012; Esat et al., 1999; Fairbanks, 1989; Peltier and Fairbanks, 2006; Yokoyama et al., 2001b] and marine sediment cores [cf., Hanebuth et al., 2000, 2009, 2011; Yokoyama et al., 2000a, 2001a]. Uncertainties of relative sea level can be produced; vertical movement in a study site, age uncertainties, and paleo-water depth estimations [cf., Bard et al., 2010, 2016; Hibbert et al., 2016; Clark and Tarasov, 2014]. To evaluate these uncertainties precisely, a comprehensive approach is required such as a selection of less tectonically active area, high- precision and resolution age-depth models, and accurate paleo-water depth reconstructions.

Previous works generally set $\delta\zeta_{tect}$ as constant through the target period, which is calculated by modern GPS data and altitude of the last interglacial coral reefs [cf., Edward et al., 1993; Chappell et al., 1996; Fairbanks, 1989; Yokoyama et al., 2001b; Peltier and Fairbanks, 2006]. $\delta\zeta_{tect}$ can change due to an abrupt tectonic event and be different between coring or drilling sites in some study sites [Bard et al., 2010, 2016; Carson and Clark, 2012]. A tectonically stable region during the target age is reliable to estimate uncertainties of relative sea-level changes precisely.

Radiocarbon dating on carbonates and organic matters is an essential dating method for late Quaternary samples [Jull et al., 2013]. Constraints on precise ages require verification of reliable ages using preservations of materials and sedimentological information of that horizon [Nakamura et al., 2016; *Chapter 2* and *3*: Ishiwa et al., 2016a, b]. Bulk organic matters in marine sediment cores are older than true ages due to the transportation time and the mixing of terrestrial and marine components [Raymond and Bauer, 2001; Kusch et al., 2010; Ohkouchi et al., 2010; Nakamura et al., 2016; Ishiwa et al., 2016a, b]. By contrast, carbonate ages of macrofossils and foraminifera indicate the reliable age of that horizon with correct local reservoir age [Nakada et al., 2016].

Paleo-water depth for a sea-level reconstruction is deduced by coral habitat range [cf., Hibbert et al., 2016; Peltier and Fairbanks, 2006; Deschamps et al., 2012] and paleoenvironmental reconstruction using faunal assemblage and sedimentological information [cf., Hanebuth et al., 2000, 2009; Yokoyama et al., 2000a, 2001a]. *Acropora palmate* is suited for reconstructing sea-level change because of its small habitat depth (~5.0 m) [Fairbanks, 1989; Peltier and Fairbanks, 2006]. However, the uncertainties of coral habitat range have been mentioned, because coral ecology derives depth distribution with the changes in salinity and temperature [Hibbert et al., 2016].

Figure 1.2-3 illustrates locations of the representative MIS 2 sea-level records, the Bonaparte Gulf [Yokoyama et al., 2000a, 2001a; De Deckker and Yokoyama, 2009], the Sunda Shelf [Hanebuth et al., 2009], the Huon Peninsula [Yokoyama et al., 2001b; Cutler et al., 2003], and the Barbados [Fairbanks, 1989; Peltier and Fairbanks, 2006]. The Bonaparte Gulf relative sea level [Yokoyama et al., 2000a, 2001a; De Deckker and Yokoyama, 2009; Nicholas et al., 2014] shows the dates after 22 cal kyr BP using marine sediment cores (Figure 1.2-4). They reassessed brackish environment during the LGM sea level minimum by further analysis [De Deckker and Yokoyama, 2009], concluding that the LGM terminated at ca. 19 cal kyr BP with a rapid sea-level rise (19 ka event). The

Sunda Shelf [Hanebuth et al., 2009] sea-level record is consistent with this 19 ka event. However, the dates show the paucity of sea-level data before ca. 22.0 cal kyr BP (Figure 1.2-4). The Huon peninsula sea-level records using uplifted corals [Yokoyama et al., 2001b; Cutler et al., 2003] demonstrate that a sea-level fall at ca. 26 cal kyr BP, which is close to the transition of MIS 3 and 2. However, records during sea level lowstands at the LGM are not observed in the Huon Peninsula (Figure 1.2-4). The Barbados sea level is a continuous record during MIS 2 [Peltier and Fairbanks, 2006]. Uplifted corals were dated using U/Th dating and paleo-water depth was deduced from coral habitat (*A.palmate*, *Montastrea annularis*, *P. asteroids*, and *Diproria* sp.). They concluded that the LGM must have occurred at 26 cal kyr BP and the amplitude of LGM sea level was -120 m (Figure 1.2-4).

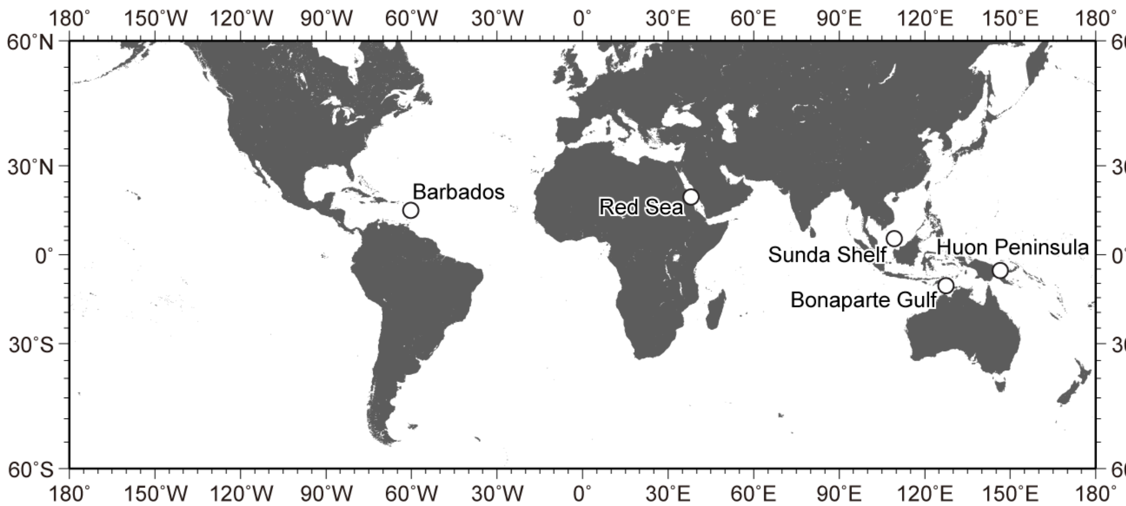

Figure 1.2-3: Locations of represented MIS 2 sea level records. The Barbados [Fairbanks, 1989; Peltier and Fairbanks, 2006], the Red Sea [Siddall et al., 2003; Grant et al., 2012, 2014; Rohling et al., 2014], the Bonaparte Gulf [Yokoyama et al., 2000a, 2001a; De Deckker and Yokoyama, 2009], the Sunda Shelf [Hanebuth et al., 2000, 2009], and the Huon Peninsula [Yokoyama et al., 2001b; Cutler et al., 2003].

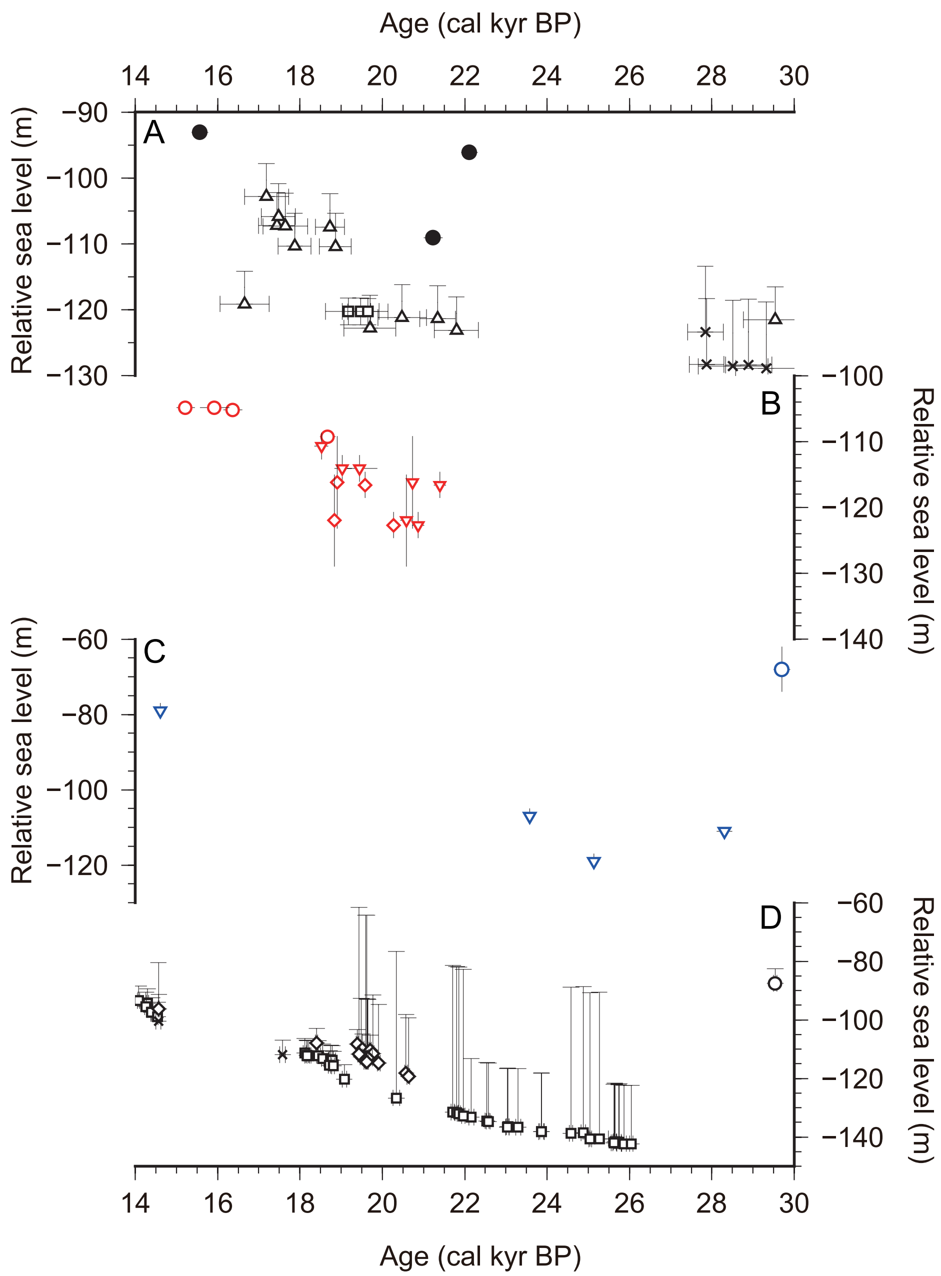

Figure 1.2-4: Relative sea level records during MIS 2. (A) The Bonaparte Gulf records [Yokoyama et al., 2000a, 2001a; De Deckker and Yokoyama, 2009; Nicholas et al., 2014]. White squares correspond to brackish, white circles to marginal marine, and black crosses to shallow marine environments [Yokoyama et al., 2000a, 2001a; De Deckker and Yokoyama, 2009]. Black circles correspond to Nicholas et al. [2014]. (B) The Sunda shelf records [Hanebuth et al., 2000, 2009]. Circles correspond to data from Hanebuth et al. [2000]. Triangles correspond to leachable organic matters and rhombuses to insoluble matters [Hanebuth et al., 2009]. (C) The Huon Peninsula records. A circle corresponds to Yokoyama et al. [2001b] and triangles to Cutler et al. [2003]. (D) The Barbados sea level records [Peltier and Fairbanks, 2006]. Symbols correspond to coring sites.

1.3 A sea-level reconstruction inferred from glacial isostatic adjustment model

Relative sea levels are different among sites due to the glacial isostatic adjustment (GIA) process (Figure 1.3-1) [Lambeck and Chappell, 2001; Yokoyama and Esat, 2011; Dutton et al., 2015]. Ice sheets covered high-latitude region during the glacial period and depressed the crust due to their weight. During the deglaciation, ice sheet melted and the crust started to uplift in the ice-covered area. This movement is still active, called as "Glacial Rebound" [Farrell and Clark, 1976; Basset et al., 2005; Yokoyama and Esat, 2011]. Water loading due to ice sheet decay causes the same phenomena in the ocean. Contributions of this effect from ice sheet and seawater are defined as "glacio isostasy" and "hydro isostasy", respectively. This redistribution of the surface load causes perturbations of the earth's rotations and gravitational field. The water on the earth's surface must remain a gravitational equipotential, governed by the redistribution of surface load.

GIA model is based on the "sea-level equation", which was firstly derived by Farrell and Clark [1976]. This model has been developed [cf., Nakada and Lambeck, 1987] to consider the effects of rotation [Milne and Mitrovica, 1996; Johnston and Lambeck, 1999; Mitorvica and Forte, 2004; Nakada and Okuno, 2003] and the migration of grounding line [Lambeck et al., 2003]. Relative sea level (RSL) at site φ and time t ($\Delta\zeta_{\mathrm{rsl}}(\varphi,\mathrm{t})$) is expressed as follows:

$$\Delta\zeta_{\mathrm{rsl}}(\varphi,\mathrm{t}) = \Delta\zeta_{\mathrm{esl}}(\mathrm{t}) + \delta\zeta_{water}^{iso}(\varphi,\mathrm{t}) + \delta\zeta_{ice}^{iso}(\varphi,\mathrm{t})$$

---------(Eq., 1.3-1)

where $\Delta\zeta_{\mathrm{esl}}(\mathrm{t})$ is ice volume equivalent sea level (ESL) and $\delta\zeta_{ice}^{iso}(\varphi,\mathrm{t})$ and $\delta\zeta_{water}^{iso}(\varphi,\mathrm{t})$ is the glacio- and hydro- isostatic contributions, respectively. Variations in $\delta\zeta_{ice}^{iso}(\varphi,\mathrm{t})$ and $\delta\zeta_{water}^{iso}(\varphi,\mathrm{t})$ are controlled by the earth model as the elastic thickness of lithosphere (H), upper-mantle viscosity (η_{um}), and lower mantle viscosity (η_{lm}) (Figure 1.3-3).

A region close to former ice sheets is "near-field" with the large effect of glacio isostasy (Figure 1.3-2). Relative sea-level curves from near-field do not relatively follow the global sea-level change since the regional isostatic effect is larger than global signal [Yokoyama and Esat, 2011]. Near-field sea-level records are useful to reconstruct the each ice sheet history and the earth structure (elastic lithosphere thickness, upper mantle viscosity, and lower mantle viscosity) [cf., Lambeck and Nakada, 1990; Lambeck 2002; Ivins and James, 2005; Lambeck et al., 2010; Peltier et al., 2015; Whitehouse et al., 2012; Argus et al., 2014; Gowan et al., 2016; Simon et al., 2016; Steffen and Kaufmann, 2005]. Since "far-field" sites are far from former ice sheets (Figure 1.3-2), that glacial isostatic effects are small, these sites are suitable to reconstruct global ice volume changes [Yokoyama et al., 2000a, 2001a; Lambeck et al., 2014; Nakada et al., 2016; Nakada and Okuno, 2016]. "Intermediate-filed" sites are located between "near-field" and "far-field" regions, being under the influence of crust bulge due to mantle flow (Figure 1.3-2) [Peltier and Fairbanks, 2006; Austermann et al., 2013].

ESL is defined as follows [cf., Lambeck et al., 2000; Lambeck et al., 2014]:

$$\Delta\zeta_{esl}(t) = -\frac{1}{\rho_o}\int \frac{1}{A_o(t)}\frac{d\Delta M_{ice}}{dt}dt$$

----------(Eq., 1.3-2)

where ΔM_{ice} is the change in ice mass at time *t* with respect to present, $A_0(t)$ is the area of ocean at t, and ρ_0 is the density of the ocean. ΔM_{ice} depends on the ice history, which is constrained using direct evidence of ice sheet, sea-level data from near- and far-field, and the instrumental data (GPS and GRACE satellite system).

Lambeck et al. [2014] constraint ESL curve using an iteration approach by ca. 1,000 far-field relative sea-level records. They also determine the earth rheology parameters (elastic lithosphere thickness and mantle viscosities). Figure 1.3-4 illustrates sea level curve of Lambeck et al. [2014], indicating that the duration of LGM is from ca.

30 to 21 cal kyr BP. A rapid ice growth of ~25 m within ca. 1,000 years is observed from 31 to 29 cal kyr BP. They suggested that gradually increased ice volume occurs from ca. 29 to 21 cal kyr BP due to the eastward and southward expansion of the Scandinavian ice sheet [Boulton et al., 2001]. The onset of deglaciation occurs from ca. 21 to 20 cal kyr BP with a ca. 10 m sea-level rise before 18 cal kyr BP.

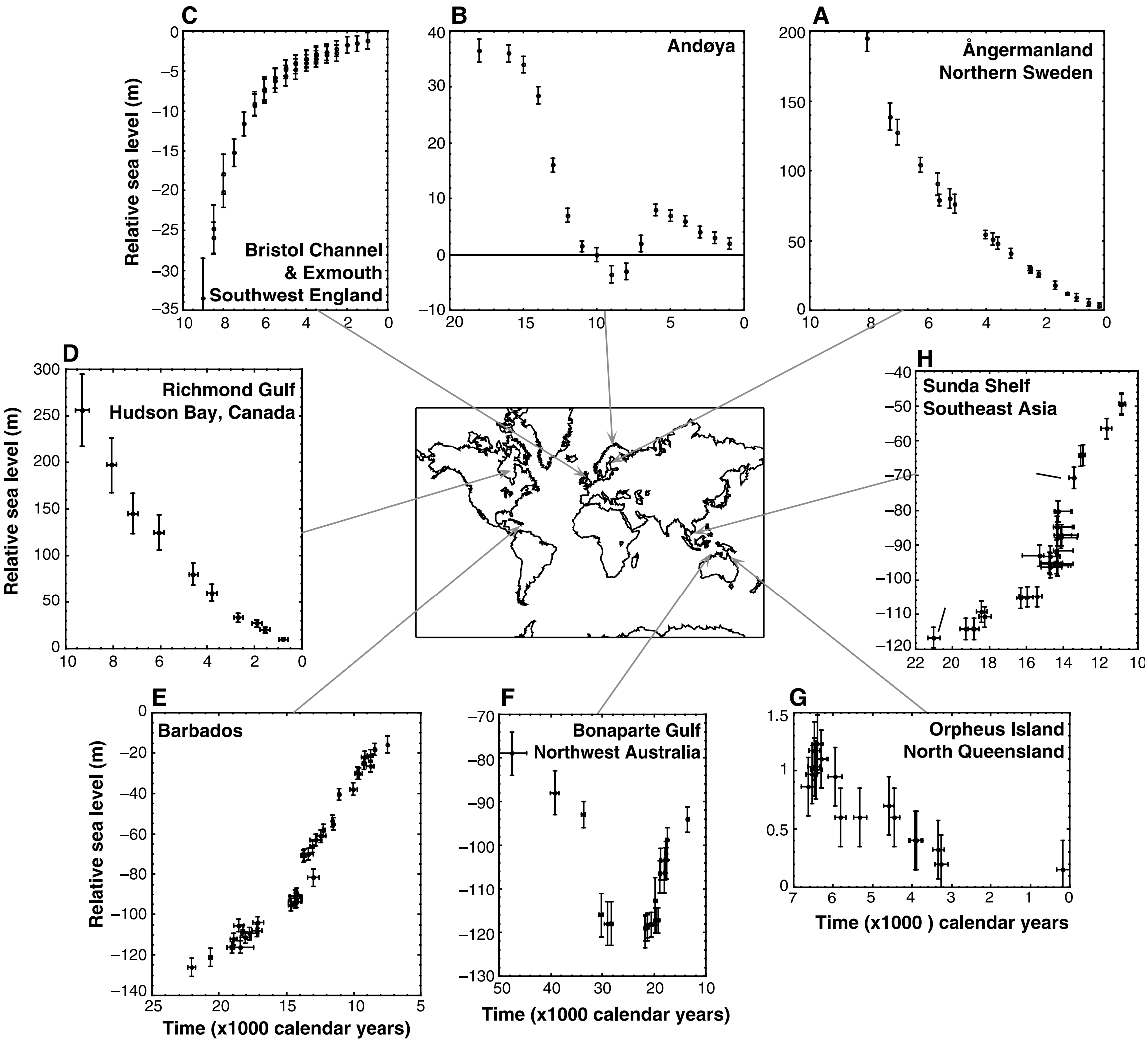

Figure 1.3-1: Observed sea level records since the timing of the LGM [Lambeck and Chappell, 2001]. The isostatic effects derive the regional differences of relative sea-level records. (A) Ångerman, Gulf of Bothnia, Sweden. (B) Andøya, Nordland, Norway. (C) South of England. (D) Hudson Bay, Canada. (E) Barbados. (F) Bonaparte Gulf, northwestern Australia. (G) Orpheus Island, North Queensland, Australia. (H) Sunda Shelf, southeast Asia. The figure and caption are referred from Lambeck and Chappell [2001].

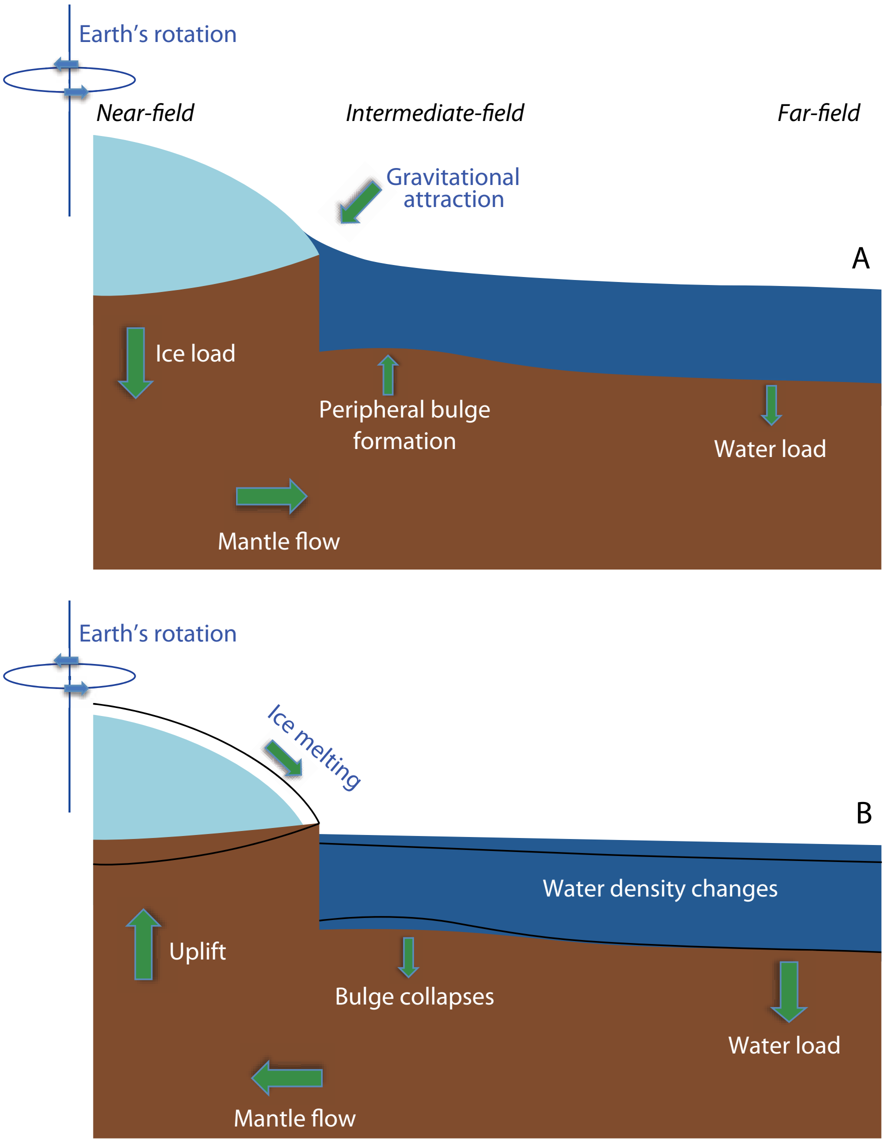

Figure 1.3-2: Sea level and ice sheet change effect to earth's surface [Yokoyama and Esat, 2011]. (A) During the period of ice sheet growth. In near field, ice load and gravitational attraction of seawater to the ice margin are observed. In intermediate field, there are crustal bulge due to mantle flow. (B) During the period of ice sheet decay. There are uplifts in near filed. Bulge collapse is observed in intermediate field. Water load occurs in far-field regions. The figure and caption are referred from Yokoyama and Esat [2011].

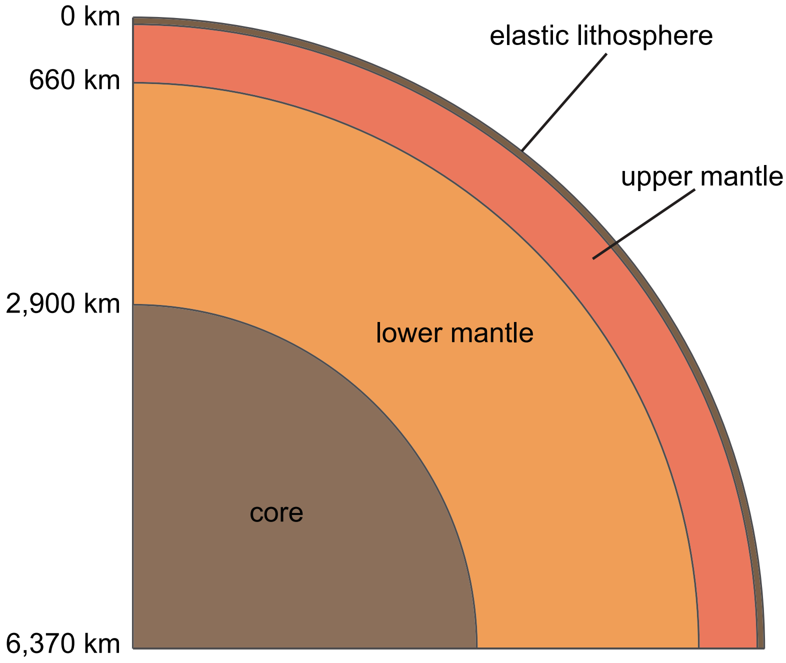

Figure 1.3-3: Cross section of the Earth structure. In GIA model process, elastic lithosphere thickness, upper mantle viscosity, and lower mantle viscosity are defined as the input parameters.

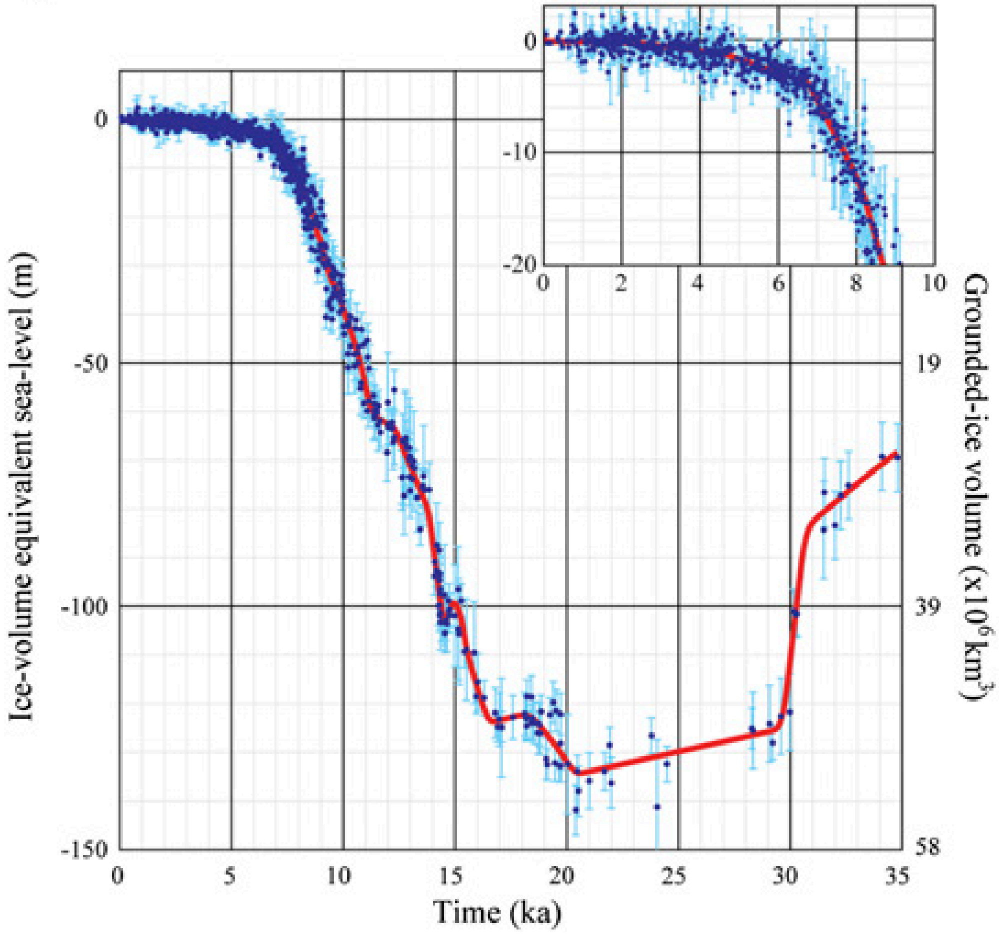

Figure 1.3-4: ESL curve from Lambeck et al. [2014]. Individual esl estimates (blue) based on far-filed sea-level data and the objective estimate of the denoised time series (red line). The inset gives an expanded scale for the last 9,000 years.

1.4 Issue of sea-level change during Marine Isotope Stage 2

The definition of LGM includes not only global sea-level minimum but also the coldest and driest part of last glacial period [Shakun and Carson, 2010; Hughes and Gibbard, 2015]. Global dust variation in high-latitude ice core records provides opportunities to define the LGM as an event with Greenland Stadial 3 (27.540–23.340 cal kyr BP) [Hughes and Gibbard, 2015]. However, this timing is not consistent with global sea-level records [Lambeck et al., 2002a, 2014; Yokoyama et al., 2000a, 2001a]. This inconsistency suggests that there is a difficulty attempting to define the global LGM (Table 1.4-1). One of the reasons is difficulty to obtain records of the pre LGM due to potential erosion during an ice volume maximum and a sea-level minimum.

In this thesis, the LGM is defined as the period of global ice volume maximum during MIS 2, corresponding to the global sea-level minimum. The number of sea-level data during MIS 2 is not enough to reconstruct global ice volume change. Lambeck et al. [2014] reported that the duration of LGM is from 30 to 21 cal kyr BP. In contrast, Peltier and Fairbanks [2006] conclude that the duration of LGM is from 26 to 16 cal kyr BP (Table 1.4-1). To detect the amplitude and timing of LGM, the accurate MIS 2 sea-level records are required, which would provide the opportunity to further understand the earth environmental system.

Table 1.4-1: The duration of LGM in some published works.

Reference	Timing	Method	Material
Yokoyama et al., 2000a, 2001a	onset before 22 cal kyr BP, terminated at 19 cal kyr BP	sea level	sediment cores in the Bonaparte Gulf
Peltier and Fairbanks, 2006	must have occurred before 26 cal kyr BP	sea level	uplifted corals in the Barbados
Clark et al., 2009	from 26 to 19 to 20 cal kyr BP	ice sheet changes	
Hanebuth et al., 2009	terminated at 19.6 cal kyr BP	sea level	sediment cores in the Sunda Shelf
Shakun and Carson, 2010	22.1±4.3 cal kyr BP	paleoclimate records	
Hughes and Gibbard, 2015	27.540–23.340 cal kyr BP	global dust records	ice cores
Lambeck et al., 2014	30–21 cal kyr BP	sea level	far-field dataset

1.5 Oceanography of the Bonaparte Gulf, northwestern Australia

The Bonaparte Gulf, northwestern Australia, is a suitable region to reconstruct relative sea-level change during MIS 2 [Yokoyama et al., 2000a; 2001a]. The shallow water depth (ca. 200 m) and gentle slope of the Bonaparte Gulf (ca. 40 km/10 m) [Lees, 1992a, 1992b] would be sensitive to sea-level changes (Figure 1.5-1), suggesting that there is the potentiality of precise sea-level reconstruction during MIS 2 period. Moreover, relative sea level in the Bonaparte Gulf reflects global ice volume change since this site is located at a far-field region [Yokoyama et al., 2000a, 2001a].

1.5.1 Geological setting

The Bonaparte Basin is located at the center of gulf, initiated at Paleozoic period [Longley et al., 2002; Courgeon et al., 2016]. The last phase of tectonic activity in the Bonaparte Gulf started during the late Miocene, which was associated with the onset of collision between the Australian continent and the Banda Arc [Haig, 2012, Bourget et al., 2014]. The rate of subsidence during late Quaternary is ca. 100 m/million year [Courgeon et al., 2016], suggesting that this rate does not affect the paleoclimate reconstructions during MIS 2.

The modern Bonaparte shelf extends up to 500 km wide. Carbonate platforms, the Londonderry, Sahul, and van Diemen Rises, have been developed with shallow depths of -30 to -70 m (Figure 1.5-1). The sediments of platforms are composed by carbonate depositions as sponges, corals, and mollusks [van Andel et al, 1967; Anderson et al., 2011; Przeslawski et al., 2014; Lavering, 1993]. These carbonate platforms were exposed during sea-level lowstands (Figure 1.5-1) [Bourget et al., 2013, 2014; van Andel et al., 1967]. Carbonate terraces and platforms contain incisions with deeper depth than -100 m, connecting the Timor Sea and the Bonaparte Basin [Courgeon et al., 2016]. Siliciclastic sediments, transported by monsoon-influenced fluvial activity, dominate the near-shore region. The amount of terrestrial sediments to the basin reaches to approximately

196×10^6 ton in each year [Lees, 1992a; Anderson et al., 2011; De Deckker et al., 2014; Nicholas et al., 2014].

The three-dimensional and two-dimensional seismic profiles combined with well data show the isolated carbonate platforms and fluvial deposition in the Bonaparte Basin [Courgeon et al., 2016]. The Bonaparte Gulf has experienced the depositional cycle, associated with the global sea-level changes. This cycle enhances the repetitions of active and drowned carbonate platforms and the deposition of terrestrial sediments [Courgeon et al., 2016].

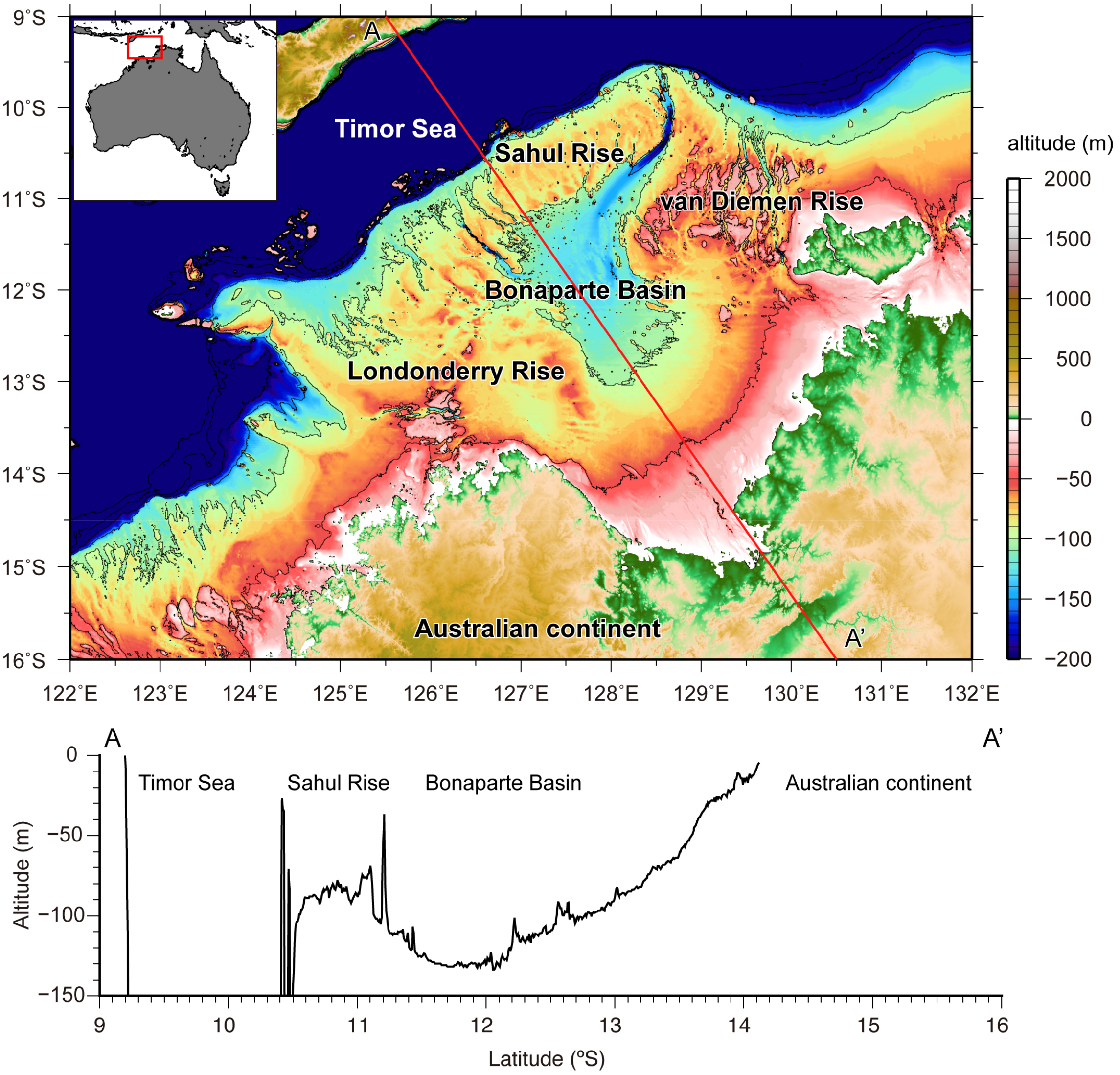

Figure 1.5-1: Map of the Bonaparte Gulf, northwestern Australia. The bathymetry data is from Whiteway [2009]. (top) The center of gulf locates the Bonaparte Basin, surrounded by carbonate terraces and platforms, the Sahul Rise, van Diemen Rise, and Londonderry Rise. The Timor Sea extends in the outer of the Bonaparte Gulf. (bottom) NW-SE transect of the Bonaparte Gulf.

1.5.2 Climate variability

Today, northwestern Australia experiences a semi-arid climate. Southeast winds prevail in the Austral summer and northwesterly winds in the Austral winter. During the Austral summer, there is strong rainfall seasonality. This precipitation pattern is the Australian monsoon [De Deckker at al., 2014; De Deckker, 2016; Gallagher et al., 2014a]. The seasonal migration of the Intertropical Convergence Zone (ITCZ) and monsoonal activity derives the distribution of rainfall (Figure 1.5-2). The intensity of rainfall has varied with the movement of the ITCZ over the past 30,000 years (Figure 1.5-2) [cf., Ding et al., 2013; Khunt et al., 2015; Mohtadi et al., 2011]. Exposure of the Sunda Shelf during global sea level lowstands influenced the hydrologic pattern in this region [DiNezio and Tierney, 2013].

The Australian monsoon was stopping or weak during the glacial period inferred from records in marine sediment cores and speleothem because of northward migration of ITCZ [Lewis et al., 2011; Partin et al., 2007; Fitzsimmons et al., 2013; Reeves et al., 2013]. This northern migration would change pattern of precipitation and dry/wet conditions in Indonesian and Australian region (Figure 1.5-3). Latitudinally transected marine sediment cores indicate that development of the Australian monsoon during the deglaciation was associated with the warming history of Antarctica (Figure 1.5-2) [Kuhnt et al., 2015]. The variation of the stable carbon compositions of vascular plant fatty acids shows the regional vegetation shift during the deglaciation in the southern Indonesia and the northern Australia, which is sensitive to changes in rainfall [Dubois et al., 2014].

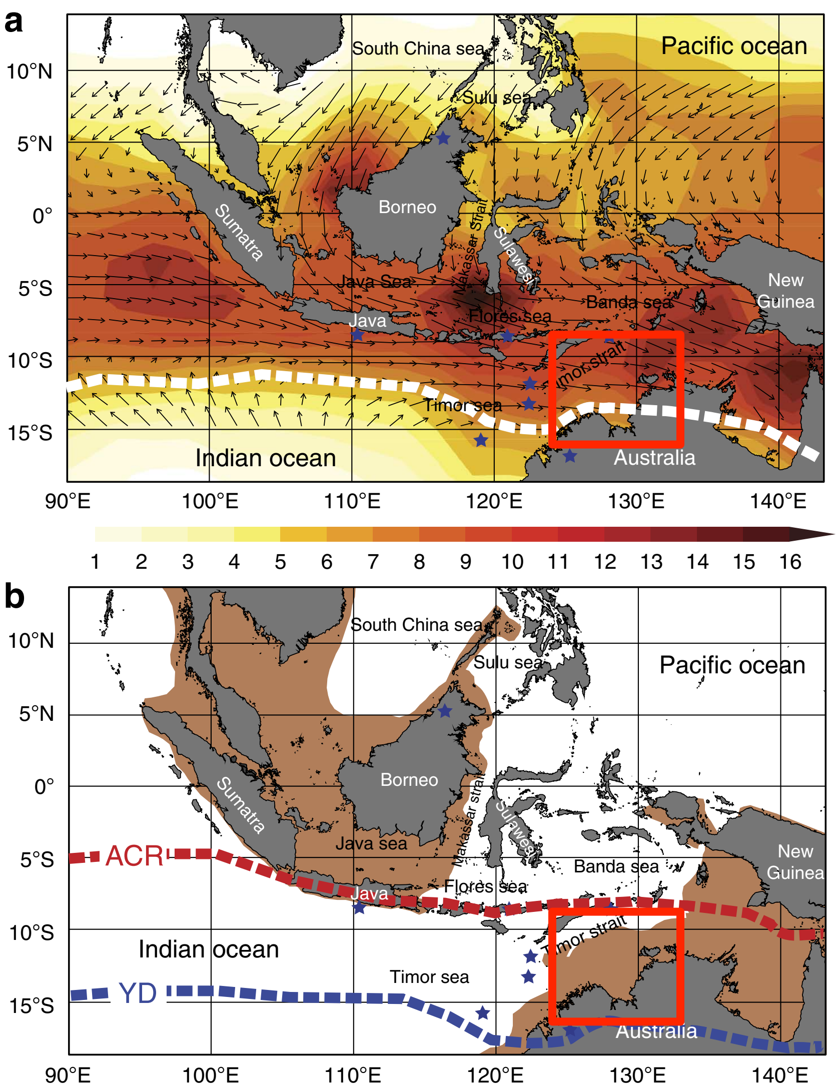

Figure 1.5-2: Displacement of the Australian monsoon in the tropical Australian region [Kuhnt et al., 2015]. Stars correspond to study sites discussed in Kuhnt et al. [2015]. Red squares correspond to the Bonaparte Gulf. (a) Modern precipitation pattern (mm/day) and wind direction in the summer. (b) Positions of the southern limit of precipitation. The ACR (Antarctic cold reversal) and YD (Younger Dryas) correspond to red and blue lines. Brown-shaded area is the exposed shelf at -120 m sea level during the LGM. The caption is modified from Kuhnt et al. [2015].

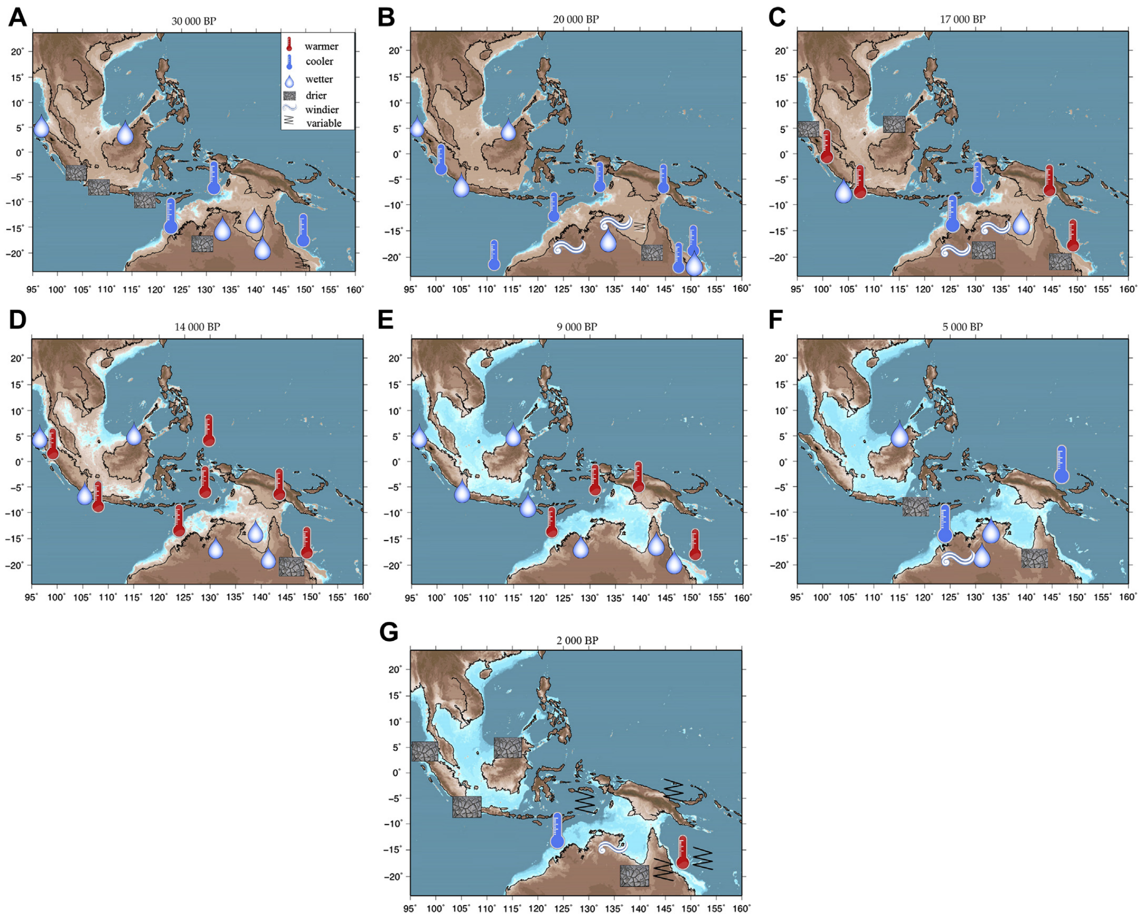

Figure 1.5-3: Climate variability in the southern Indonesia and northern Australia reconstructed from various archives [Reeves et al., 2013].

1.6 Research objective and thesis structure

A further understanding of global and regional climate requires the precise MIS 2 sea-level reconstruction since sea-level change provides global ice volume change and regional exposure history in the continental shelf. However, a relative sea-level record during MIS 2 is not reconstructed well due to its large uncertainty and insignificant number of the dataset. This derives the discrepancy of ice volume change history during the LGM [cf., Peltier and Fairbanks, 2006; Lambeck et al., 2014; Clark and Tarasov, 2014].

The main objective of this study is to improve ice volume history during MIS 2 through a reconstruction of relative sea level in the Bonaparte Gulf. In *Chapter 2* (cf., *Ishiwa et al., 2016a*), the sedimentary environment in the Bonaparte Gulf will be discussed since the understanding of regional setting is necessary to reconstruct the precise relative sea-level change. In *Chapter 3* (cf., *Ishiwa et al., 2016b*), relative sea level records during MIS 2 will be presented using marine sediment cores in the Bonaparte Gulf. In *Chapter 4*, the new ESL curve will be proposed, which is based on the relative sea-level curve from the Bonaparte Gulf, and be evaluated by comparison with other relative sea-level records. Finally, in *Chapter 5*, the new ESL curve, which is a key finding in this dissertation, will be discussed in comparison with other ESL curves. In addition, future perspectives in the ice volume fluctuations during MIS 2 will also be suggested.

Chapter 2 Sedimentary environmental change in the Bonaparte Gulf during Marine Isotope Stage 2

本章は，5 年以内に雑誌等で刊行予定のため一部非公開.

Abstract

An understanding of sedimentary environments driven by paleoclimatological processes derives an accurate reconstruction of past sea-level change. The Bonaparte Gulf is among the widest in the world, ranging to 500 km, with shallow carbonate terraces and platforms that were exposed during periods of lower sea level. The dominant sediments type has switched between carbonate and siliciclastic over a sea-level cycle. However, the mechanism of sedimentary environmental change in the Bonaparte Gulf is not clearly understood. The Bonaparte Gulf is known as one of the largest tidal range regions, up to 6.0 m, equivalent to the volume of Greenland Ice Sheet. An evaluation of past tide is required to reconstruct sea-level change precisely. In this chapter, I present a record of sedimentary environmental change from ca. 24 to 35 cal kyr BP that is related to sea-level variability and exposure of carbonate terraces and platforms, combined with a paleo-tidal model. Multi-proxy data from a marine sediment core shows a sea-level change induced switch in the sedimentary environment from siliciclastic to carbonate-dominated sedimentation during the last glaciation. Radiocarbon ages constrain the timing of this switch to ca. 26 cal kyr BP, associated with a local sea-level fall to -90 m. The influence of tide to the sedimentary environment was negligible due to the protection of carbonate terraces and platforms from wave activities of the Timor Sea. During sea level lowstands, the sedimentary environment in the Bonaparte Gulf was semi-enclosed from the Timor Sea and the depositions in the basin had been enhanced.

2.1 Introduction

The Bonaparte Gulf is a broad continental shelf with a water depth shallower than ca. 200 m (Figure 2.1-2) [Bourget et al., 2013, 2014]. Potentially, the sedimentary environment in the Bonaparte Gulf has changed due to shallow water depth (ca. -200 m), which is sensitive to sea-level change with the amplitude of ca. -130 m during the glacial-interglacial cycle. Researches on a sea-level reconstruction require better understanding of sedimentary environmental changes since precise age-depth models and paleoenvironmental reconstructions would provide an accurate relative sea-level record [cf., Yokoyama et al., 2000a, 2001a; De Deckker and Yokoyama, 2009]. Moreover, mixed siliciclastic-carbonate sedimentary environment in low-latitude and semi-enclosed marginal marine environments provides information on the mechanism of paleoclimatic and hydrologic change [cf., Bahr et al., 2005; Isaack et al., 2016; Soulet et al., 2011]. However, our understanding of late Quaternary evolution of the Bonaparte sedimentary environment is much less constrained.

In some basins, large tidal ranges are observed due to a node of the tide in the mouth of the basin. In this case, the resonant period (T) can be calculated as follows:

$$T = \frac{4l}{\sqrt{gd}}$$

----------(Eq. 2.1-1)

where l is the length of the basin, g is the gravitational acceleration, and d is the average depth of basin. In the Bonaparte Gulf, l is ca. 380 km, and d is ca. 80 m [Louis and Radok, 1975]. For these values, T is calculated to ca. 15 hours. This almost corresponds to the duration of the semidiurnal constituents (Table 2.1-1), indicating that there are large tidal ranges in the Bonaparte Gulf.

The large tidal range in near shore region is observed in the Bonaparte Gulf (Table 2.1-2) with the amplitude of up to 6 m. This value is equivalent to the volume of Greenland Ice Sheet. Global tideal model shows increasing trend from modern to the

LGM in the northwestern Australian region (Figure 2.1-2) [Griffiths and Peltier, 2009]. However, the resolution of bathymetry around the Bonaparte Gulf is not enough to detect the difference of tidal range between sea-level highstands and lowstands

Here I document evidence of environmental change in the Bonaparte Gulf due to exposure of these carbonate terraces and platforms during MIS 2. The Bonaparte Gulf is a "far-field" [cf, Yokoyama and Esat, 2011], tectonically stable site extremely suitable for global sea-level reconstruction [Yokoyama et al., 2000a; 2001a; De Deckker and Yokoyama, 2009; Ishiwa et al., 2016b]. I also describe the sedimentary consequences of past environmental change from a marine piston core (KH11-1-PC01) using Ca/Ti ratios, total organic carbon (TOC) and total nitrogen (TN), constrained by radiocarbon dating. Tidal evolution associated with sea-level change is also shown using the two-dimensional paleotidal model [Uehara, 2012] and discussed with the sedimentary environmental change.

Table 2.1-1: Summary of tidal constituent discussed in this chapter [Shennan et al., 2015]. The Bonaparte Gulf has the large tidal range, caused by the semi diurnal tide (M2 and S2).

constituent	period (hour)	
M2	12.42	Lunar, principal
K1	23.93	Solar, Lunar, declination
S2	12	Solar, principal
O1	25.82	Lunar, declination

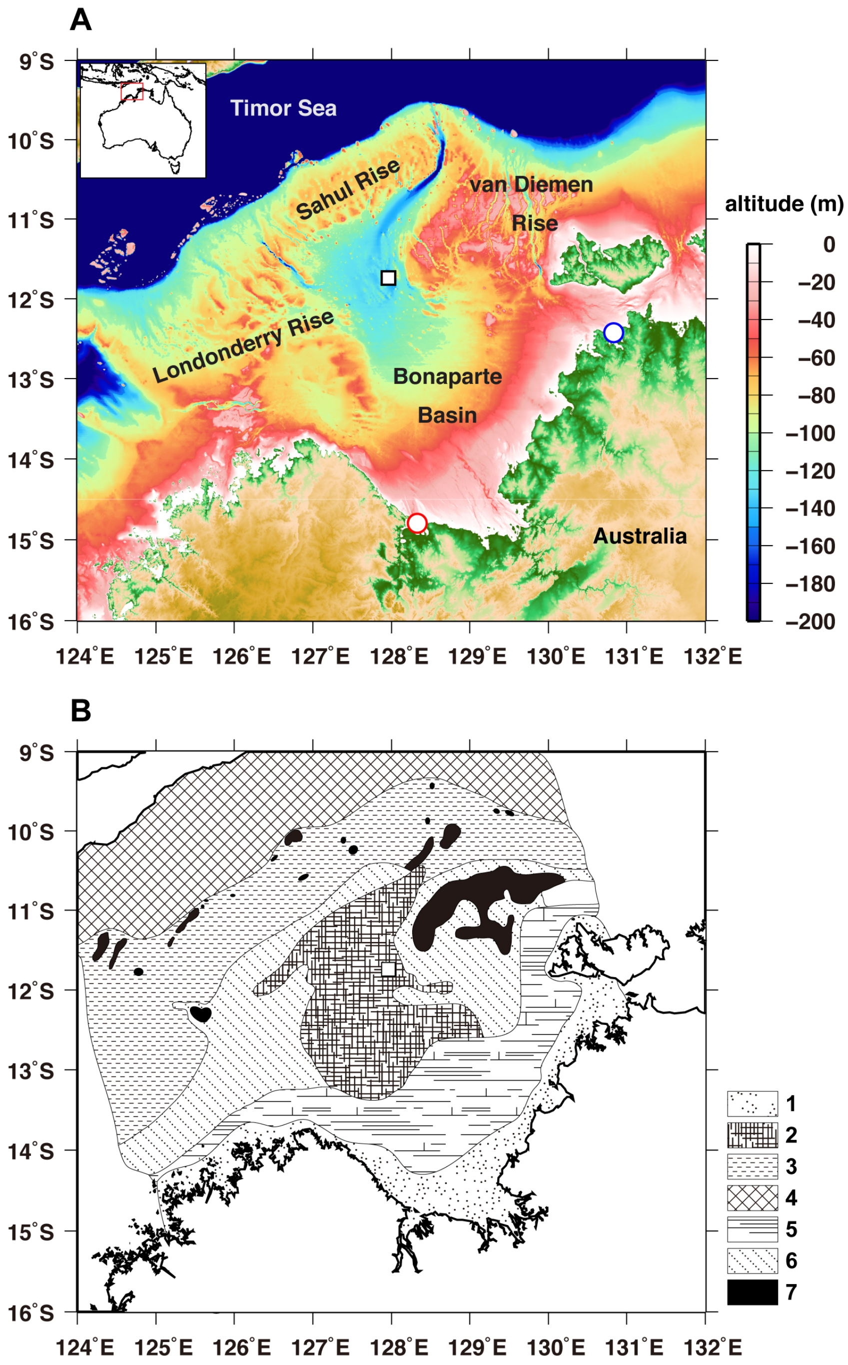

Figure 2.1-1: Map of Bonaparte Gulf, northwestern Australia. (A) The location of core site KH11-1-PC01 (white square), bathymetry and named seabed features are referred to in the text. Bathymetric data is from Whiteway [2009]. The locations of Lacrosse Island and Darwin show red and blue circles, respectively. (B) Distribution of surface sediments, modified from van Andel et al. [1967]. 1: recent near-shore sediments, 2: calcareous silty clays of Bonaparte Depression, 3: shelf-edge foraminiferal calcilutites and calcarenites, 4: Timor Trough silty clay and calcilutites, 5: relict transgressive quartzose calcarenites, 6: relict transgressive calcarenites, 7: bank facies. Legends refer to van Andel et al. [1967].

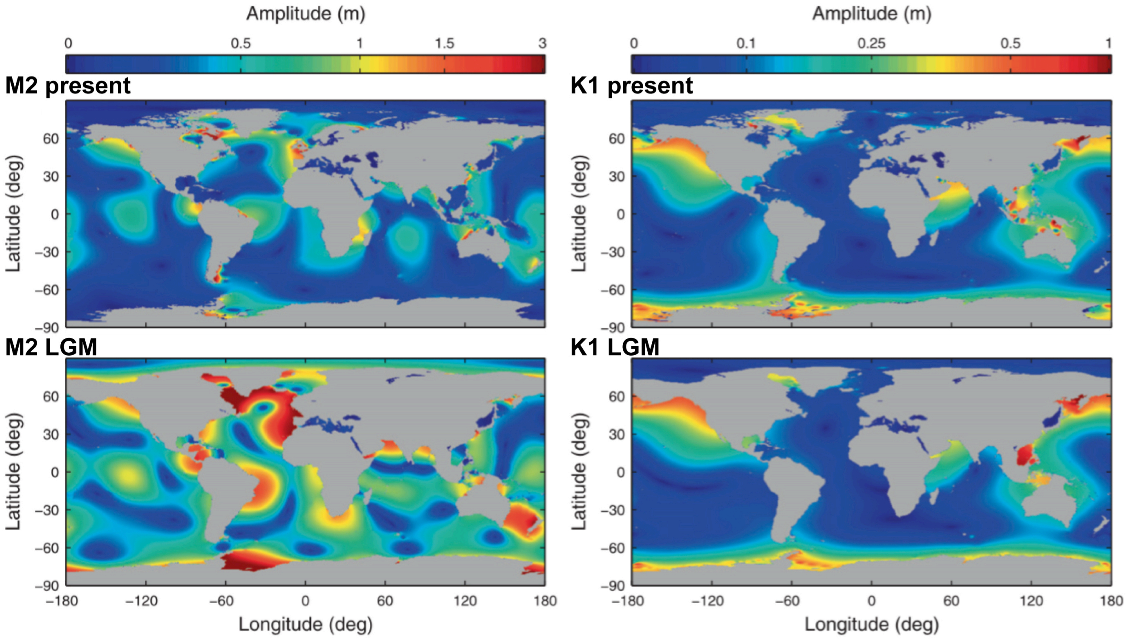

Figure 2.1-2: Tidel amplitude of M2 and K1 at present and LGM from TPXO 6.2 dataset and Global Tidal model [Griffiths and Peltier, 2009]. The figure and caption are modified from Griffiths and Peltier [2009].

Table 2.1-2: Tide of Darwin and Lacrosse Island in the Bonaparte Gulf in November 2016 [http://www.bom.gov.au/ntc/]. Locations are shown in Figure 2.1-1.

Date	Darwin			Lacrosse Island		
FRI 11 NOV	HIGH	2:41 AM	5.91 m	HIGH	2:33 AM	5.41 m
	LOW	9:40 AM	2.60 m	LOW	9:11 AM	1.77 m
	HIGH	3:40 PM	5.72 m	HIGH	3:31 PM	5.04 m
	LOW	9:42 PM	2.82 m	LOW	9:17 PM	2.36 m
SAT 12 NOV	HIGH	3:43 AM	6.27 m	HIGH	3:28 AM	5.64 m
	LOW	10:29 AM	1.92 m	LOW	9:51 AM	1.20 m
	HIGH	4:36 PM	6.45 m	HIGH	4:17 PM	5.72 m
	LOW	10:39 PM	2.48 m	LOW	10:13 PM	2.09 m
SUN 13 NOV	HIGH	4:30 AM	6.65 m	HIGH	4:09 AM	5.83 m
	LOW	11:13 AM	1.25 m	LOW	10:26 AM	0.72 m
	HIGH	5:27 PM	7.11 m	HIGH	4:58 PM	6.30 m
	LOW	11:28 PM	2.19 m	LOW	10:59 PM	1.92 m
MON 14 NOV Full Moon	HIGH	5:12 AM	6.98 m	HIGH	4:47 AM	5.95 m
	LOW	11:55 AM	0.68 m	LOW	11:01 AM	0.35 m
	HIGH	6:14 PM	7.62 m	HIGH	5:39 PM	6.72 m
				LOW	11:41 PM	1.87 m
TUE 15 NOV	LOW	12:11 AM	2.00 m	HIGH	5:23 AM	5.99 m
	HIGH	5:51 AM	7.20 m	LOW	11:36 AM	0.14 m
	LOW	12:35 PM	0.29 m	HIGH	6:21 PM	6.95 m
	HIGH	6:59 PM	7.93 m			
WED 16 NOV	LOW	12:52 AM	1.94 m	LOW	12:22 AM	1.93 m
	HIGH	6:28 AM	7.29 m	HIGH	6:02 AM	5.95 m
	LOW	1:14 PM	0.12 m	LOW	12:16 PM	0.11 m
	HIGH	7:43 PM	8.02 m	HIGH	7:07 PM	7.02 m
THU 17 NOV	LOW	1:32 AM	2.01 m	LOW	1:04 AM	2.06 m
	HIGH	7:06 AM	7.21 m	HIGH	6:45 AM	5.84 m
	LOW	1:55 PM	0.21 m	LOW	12:58 PM	0.27 m
	HIGH	8:24 PM	7.90 m	HIGH	7:55 PM	6.97 m

2.2 Materials

Core KH11-1-PC01 was recovered from a water depth of 140 m during the KH11-1 cruise of R/V Hakuho-Maru during January and February 2011 (Figure 2.1-1). The top 600 cm interval of core KH11-1-PC01 (core recovery length: 951 cm) was analyzed as it is within the range of radiocarbon dating. Well-preserved macrofossils (primarily bivalves) were collected for radiocarbon dating.

2.3 Methods

2.3.1 Physical properties and geochemical analysis

Color reflectance was measured at 2-cm intervals after splitting the cores on a ship using a Minolta CM-2002 photospectrometer. At the same time, magnetic susceptibility was measured at 2-cm intervals using a Bartington Instruments MS2C system.

TOC and TN were measured using an EA-IRMS (Elemental Analysis - Isotope Ratio Mass Spectrometry: Flash EA 1112 and Delta plus Advantage) at the Center for Advanced Marine Core Research, Kochi University (Figure 2.3-1) [cf., Ishiwa et al., 2016b; Nakamura et al., 2016; Riethdorf et al., 2015]. Bulk sediments were treated with 3 M HCl to remove inorganic carbonate. Split-core scanning X-ray fluorescence (XRF) analysis was then conducted at a 1-cm interval using the TATSCAN-F2 at the Center for Advanced Marine Core Research [Sakamoto et al., 2006]. XRF core scanner analysis was affected by the split-core surface condition and water content, especially for the light elements [Kido et al., 2006; Nakamura et al., 2016]. Hence, I discuss the variation of relatively heavy elements, calcium (Ca), potassium (K), manganese (Mn), iron (Fe) and titanium (Ti). For example, the flux of Ca, and Ti is calculated as follows:

$$\mathrm{MAR} = \mathrm{DBD} \times \mathrm{LSR}$$

----------(Eq., 2.3-1)

$$\text{Ca (Ti) flux} = \text{MAR} \times \text{Ca (Ti) (counts)}$$

----------(Eq., 2.3-2)

where MAR is the mass accumulation rate ($g/cm^2 \cdot yr$), DBD is the dry bulk density (g/cm^3), and LSR is the liner sedimentation rate (cm/yr).

Radiocarbon dating was performed on marine macrofossils and bulk sediment organic matter. Macrofossils were etched by 10 M HCl to remove secondary and contaminating calcium carbonate [Yokoyama et al., 2016a]. Bulk sediments were pretreated twice in 3 M HCl for 12 hours to digest inorganic calcium carbonate [cf., *Chapter 3*; Ishiwa et al., 2016b]. I followed the methods of Yokoyama et al. [2007] and measured the graphite by the Single Stage Accelerator Mass Spectrometry (Figure 2.3-1) [Yokoyama et al., 2016b] and the Micro Analysis Laboratory Tandem Accelerator at the University of Tokyo.

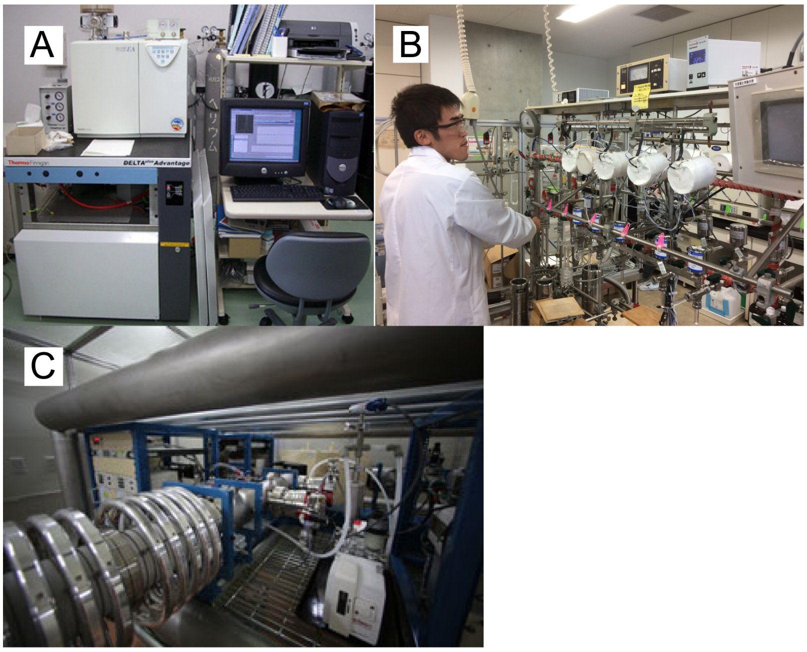

Figure 2.3-1: Photo of EA-IRMS, gratification, and AMS. (A) EA-IRMS (Elemental Analysis - Isotope Ratio Mass Spectrometry: Flash EA 1112 and Delta plus Advantage) at the Center for Advanced Marine Core Research, Kochi University. (B) Gratification systems at Atmosphere and Ocean Research Institute, The University of Tokyo. (C) Single Stage AMS at Atmosphere and Ocean Research Institute, The University of Tokyo.

2.3.2 Age-depth model

Calendar ages were calculated using Oxcal [Ramsey and Lee, 2013] with Marine 13 and Intcal 13 [Reimer et al., 2013] as calibration curves for macrofossils and organic matter ages. The local reservoir correction, ΔR, is undefined in the Bonaparte Gulf but expected to be minor [cf., Bowman, 1985; O'Connor et al., 2010]. Thus, we made no local correction consistent with previous works [Yokoyama et al., 2000a, 2001a; cf., Ishiwa et al., 2016b].

The age-depth model of KH11-1-PC01 was constrained using the BACON model [Blaauw and Christen, 2011] based on macrofossil ages since organic matter ages are affected by the transportation time of terrestrial components [cf., Nakamura et al., 2016; *Chapter 3*, Ishiwa et al., 2016b]. This model uses Bayesian analysis and the Monte Carlo methods to constrain the smoothing age depth model using the R statistical software package [cf., De Vleeschouwer et al., 2012; Shanahan et al., 2012].

2.3.3 Calculation for exposure percentage in the Bonaparte Gulf

The area of carbonate terraces and platforms in the Bonaparte Gulf exposed during lower sea level was calculated using the bathymetric dataset from Whiteway [2009]. The data were interpolated to a uniform resolution of 0.5 minutes latitudinally and longitudinally. I calculated the area of exposure along the sea-level curve and set the exposure percentage to 0% at relative sea level = 0 m and to 100% at relative sea level = -120 m. This percentage was calculated at a 5-m interval.

2.4 Results

2.4.1 Lithology and Physical properties

The interval from 600 to 560 cmbsf (cm below sea floor) of core KH11-1-PC01 is silty clay with mm-scale shell fragments. Fine sand is present from 560 to 520 cmbsf and silty clay is from 520 to 510 cmbsf with shell fragments, foraminifera and nannofossils (as noted in shipboard smear slides). Fine sand is present from 510 to 490 cmbsf and silty clay with shell fragments, and nannofossils from 490 to 60 cmbsf. The upper 60 cm of the core is silt and clay with shell fragments and bioturbation. Color reflectance (b*) values gradually increase from 1 to 9 in the uppermost 300 cm with a slight shift at 200 cmbsf, indicating an increasing yellow component. A relatively large increase in b* occurs at 30 cmbsf (Figure 2.4-1). Magnetic susceptibility (MS) shows a slight decrease from 7 to 4 SI 10^{-6} at 200 cmbsf with a maximum of 11 SI 10^{-6} at 10 cmbsf. In the upper 10 cm, the MS decreases to 0 SI 10^{-6} (Figure 2.4-1).

2.4.2 XRF core scanning and geochemical analysis

Ca counts are constantly at 600,000 from 600 to 200 cmbsf, increasing to ca. 800,000 counts at 180 cmbsf (Figure 2.4-1). Decreased Ca is observed at 70 cmbsf. From 30 cmbsf to the core top, Ca decreases to 400,000 counts. Ti gradually decreases from 600 to 200 cmbsf, sharply decreasing to 20,000 counts at ca. 200 cmbsf (Figure 2.4-1). There is a peak of ca. 25,000 counts from 30 cmbsf to the core top.

TOC is ca. 0.7% from 600 to 200 cmbsf, sharply increasing to 1.5% at 180 cmbsf with a peak of ca. 0.8% at 510 cmbsf (Figure 2.4-1). TOC is variable in the upper 40 cm of the core. C/N ratios reach a maximum of ca. 15 at 510 cmbsf, then maintain a value of ca. 9 through the depth interval of 500–180 cmbsf, above which values are relatively constant at ca. 13 (Figure 2.4-1). In the upper 60 cm, ratios decrease upwards to the core top.

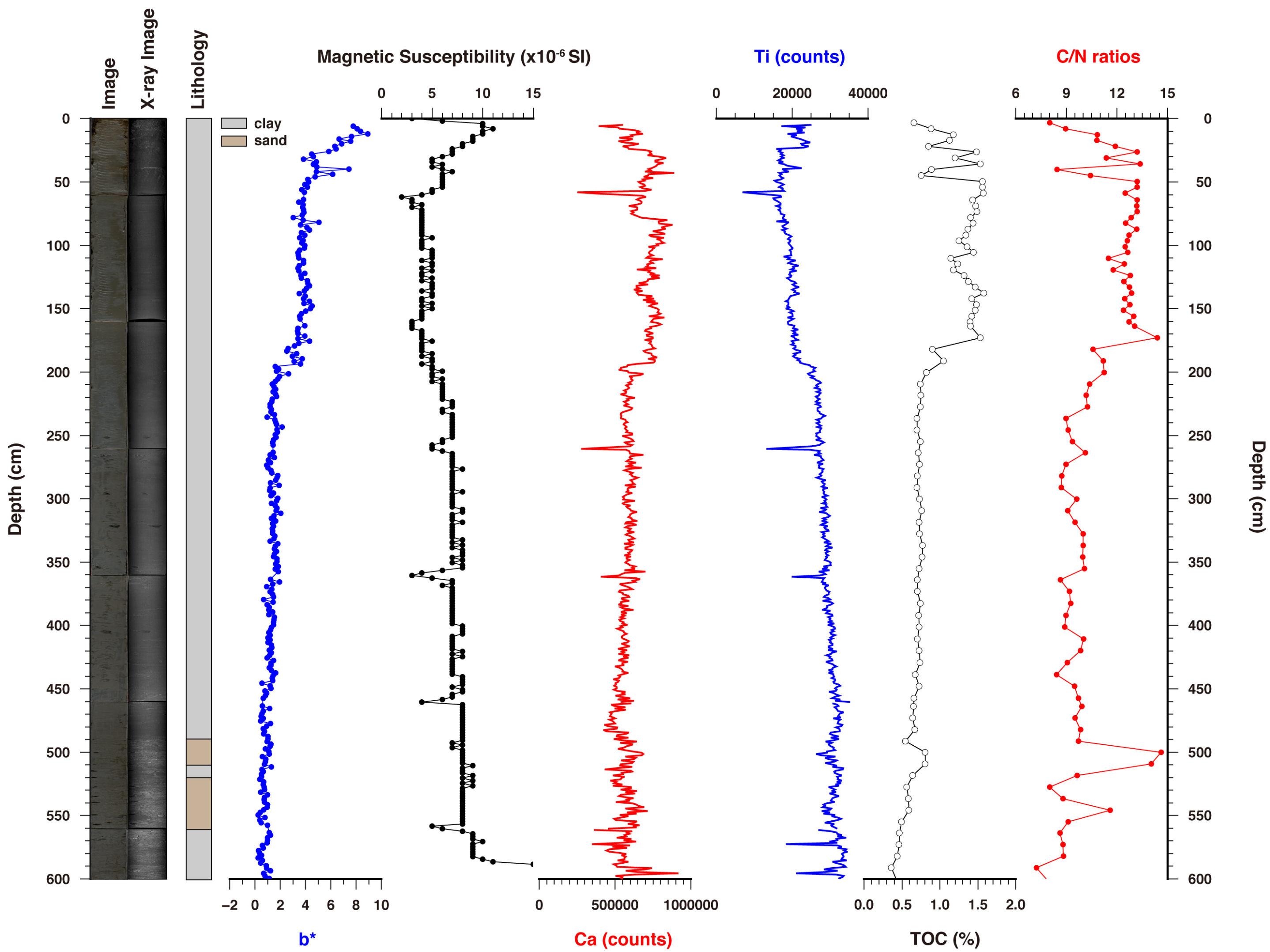

Figure 2.4-1: Image of core KH11-1-PC01, X-ray image, lithology, color reflectance (b*), magnetic susceptibility, Ca, Ti, TOC, and C/N ratios.

2.4.3 Radiocarbon dating

Table 2.4-1 and 2.4-2 summarize the results of radiocarbon dating and Figure 2.4-2 shows the age-depth relationship. Macrofossils dates show the range from ca. 35 to 24 cal kyr BP and bulk organic matter from ca. 37 to 25 cal kyr BP during the interval of 600 to 60 cmbsf. The upper 60 cm is either disturbed by coring or winnowed by tidal currents [http://www.bom.gov.au/australia/tides/] and pockmark activity [Nicholas et al., 2014]. X-ray image shows the accumulation of high-density materials in this interval, which is consistent with the high tidal energy in the Bonaparte Gulf during sea-level highstands (see *section 2.5.3*). The ages in this interval are not interpreted here (Figure 2.4-2). Below 60 cmbsf, the age-depth model is well constrained with an offset between macrofossils and organic matter ages [cf., *Chapter 3*: Ishiwa et al., 2016b]. The average value of this offset is ca. 800 ^{14}C yr within the period from ca. 35 to 25 cal kyr BP and ca. 1,200 ^{14}C yr with the period from ca. 25 to 24 cal kyr BP. The average sedimentation rate is 0.47 m/kyr for the period from ca. 35 to 25 cal kyr BP and 0.75 m/kry for the period from ca. 25 to 24 cal kyr BP.

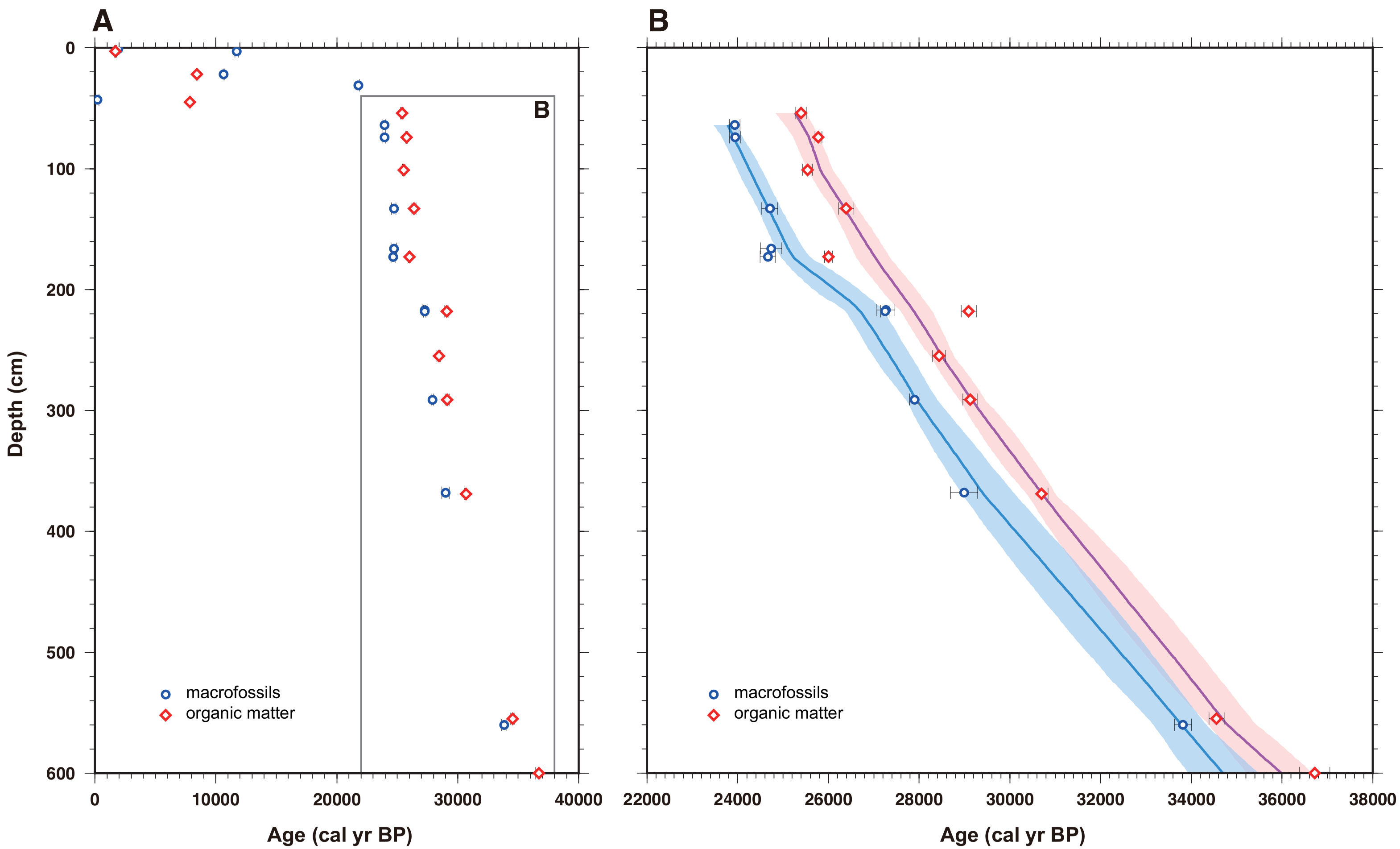

Figure 2.4-2: The age-depth relationship of core KH11-1-PC01. (A) Calendar ages for macrofossils (blue) and organic matter (red). The errors are 2 sigma. (B) Expanded view of the age-depth model in 22–38 cal kyr BP. Line is the mean value of the BACON model [Blaauw and Christen, 2011] and the shade is the minimum and maximum range of BACON model.

Table 2.4-1: Age results of macrofossils in core KH11-1-PC01. Data are calculated by Marine13 [Reimer et al., 2013]. "YAUT-" is a laboratory number of the Single Stage Accelerator Mass Spectrometry at The University of Tokyo. "B274" is a laboratory number of the Micro Analysis Laboratory Tandem Accelerator at The University of Tokyo.

Lab. No.	Material	Depth (cm)	^{14}C age (BP)	Calendar age (cal BP) 1 σ	Calendar age (cal BP) 2 σ
YAUT-01960	bivalves	1	2320±30	1940±40	1940±90
YAUT-01960	bivalves	3	10510±40	11730±140	11670±260
YAUT-01960	bivalves	22	9750±40	10650±50	10660±110
YAUT-01960	bivalves	31	18370±50	21770±100	21750±200
B274	coral	43	590±130	200±140	-
YAUT-01961	bivalves	64	20290±70	23930±120	23920±250
YAUT-01961	bivalves	74	20290±70	23940±120	23930±250
YAUT-01961	bivalves	133	20940±70	24710±180	24730±320
B274	bivalves	166	20950±140	24740±240	24760±430
YAUT-01964	bivalves	173	20910±70	24660±170	24690±310
B274	bivalves	217	23320±210	27270±200	27160±450
YAUT-01961	bivalves	218	23280±70	27250±100	27240±200
YAUT-01962	bivalves	291	24280±90	27890±100	27920±220
B274	barnacle	368	25330±280	28990±300	29020±610
B274	gastropod	560	30060±230	33820±190	33820±410
B274	bivalves	603	35020±550	39160±580	39270±1280

Table 2.4-2: Age results of organic matter in core KH11-1-PC01. Data are calculated by Intcal 13 [Reimer et al., 2013]. "YAUT-" is a laboratory number of the Single Stage Accelerator Mass Spectrometry at The University of Tokyo.

Lab. No.	Depth (cm)	^{14}C age (BP)	Calendar age (cal BP) 1 σ	Calendar age (cal BP) 2 σ
YAUT-003718	3	1790±30	1700±80	1720±100
YAUT-003906	22	7650±30	8430±20	8450±60
YAUT-003719	45	7040±70	7870±70	7840±140
YAUT-012705	54	21040±80	25400±120	25390±230
YAUT-003907	74	21450±60	25780±80	25770±150
YAUT-004007	101	21180±70	25540±110	25510±220
YAUT-003720	133	22200±110	26390±170	26440±350
YAUT-003721	173	21780±100	26000±90	26010±200
YAUT-003722	218	25060±110	29090±170	29110±320
YAUT-014534	255	24370±90	28440±150	28420±280
YAUT-004008	291	25090±90	29120±160	29140±300
YAUT-003723	369	26360±130	30700±150	30660±300
YAUT-003724	555	30600±150	34560±170	34530±330
YAUT-003725	600	32810±200	36720±330	36930±680

2.4.4 Exposure of carbonate terraces and platforms in the Bonaparte Gulf

Figure 2.4-3 shows the calculated percentage of exposure and the rate of sea-level change from 0 m to -120 m in 5 m increments. During sea level lowstands, the proportion of carbonate terraces and platforms exposed in the Bonaparte Gulf ranged from 25% when sea level was at -60 m to in excess of 90% when sea level fell below -100 m. The rate of change from -70 to -90 m is greater than 1.5 %/m. The maximum rate of change is at -80 m.

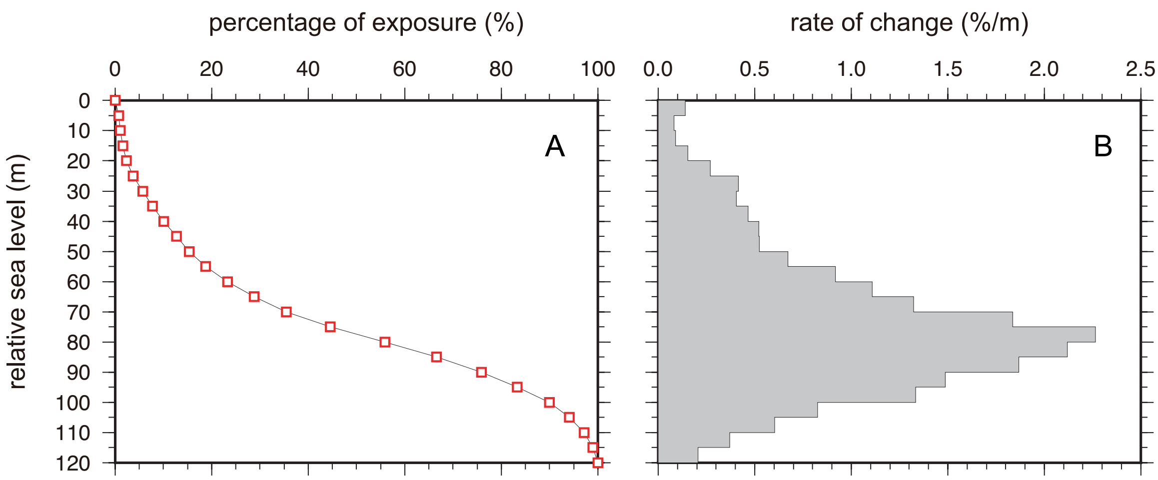

Figure 2.4-3: (A) Proportion (%) of carbonate platform area in the Bonaparte Gulf exposed at lower sea levels; (B) Rate of change in proportional area of the platforms exposed at sea level fall.

2.5 Discussion

2.5.1 Sedimentary environmental change during late Quaternary

Biogenic or precipitated carbonate shows high Ca-intensities with an inverse relationship to K-, Fe-, Mn-, and Ti- intensities that are correlated with siliciclastic components [cf., Bahr et al., 2005; Kuhnt et al., 2015]. Ca/Ti, Ca/K, Ca/Mn, and Ca/Fe ratios all exhibit a similar pattern of variability (Figure 2.5-1). Thus I focus on Ca/Ti ratios, which is less sensitive to changes in redox state. I suggest that calcium variation represents changes in biogenetic carbonate flux from the carbonate terraces and platforms of the Bonaparte Gulf. The Ca flux after 25 cal kyr BP is much higher than before 27 cal kyr BP, indicating a carbonate flux increase caused by exposure of the carbonate platforms during lower sea level at ca. 26 cal kyr BP (190 cm) (Figure 2.5-2). In addition, I use Ti variation to represent terrestrial sediment flux, derived from clay minerals [cf., Gingele et al., 2001; Gingele and De Deckker, 2003]. Magnetic susceptibility values decrease from 27 to 25 cal kyr BP (Figure 2.5-3). This pattern likely reflects the dilution by sediments dominated by biogenetic carbonate with low magnetic susceptibility.

Variation in terrestrial input would be related to changes in TOC flux and C/N ratios [cf., Yu et al., 2010; Mackie et al., 2005, 2007; *Chapter 3*: Ishiwa et al., 2016b]. Terrestrial sediment supply increases after ca. 26 cal kyr BP, as indicated by the increased TOC, C/N ratios, and sedimentation rate (Figures 2.5-2 and 2.5-3). Increasing terrestrial material during this time would make mixed marine-terrestrial organic matter older, increasing the offset from macrofossil ages (Figure 2.4-2). Additionally, mass accumulation rate calculated by the BACON model supports the carbonate terraces and platforms exposure after ca. 26 cal kyr BP (Figure 2.5-2).

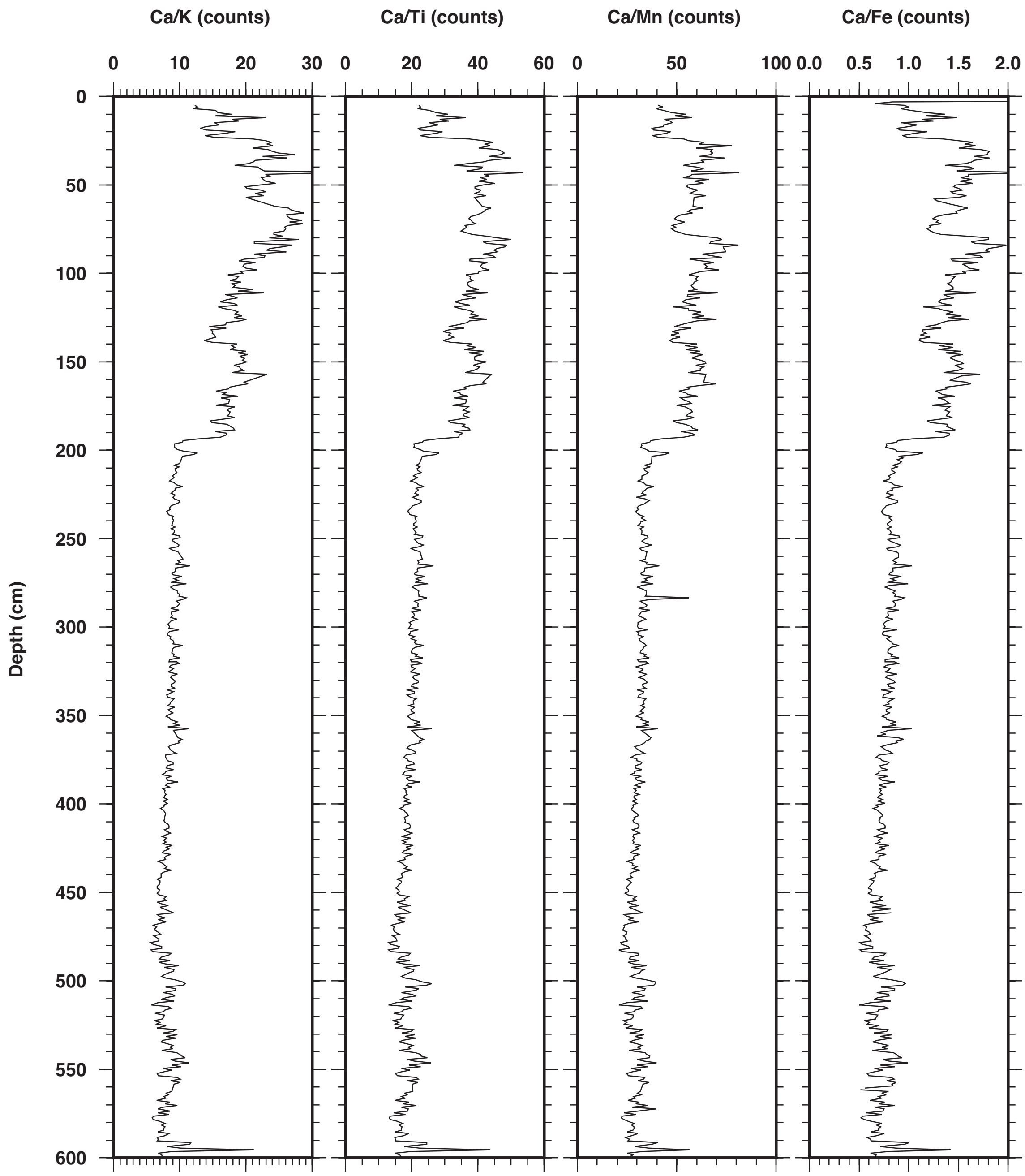

Figure 2.5-1: Ca/K, Ca/Ti, Ca/Mn, and Ca/Fe variation from XRF core scanner.

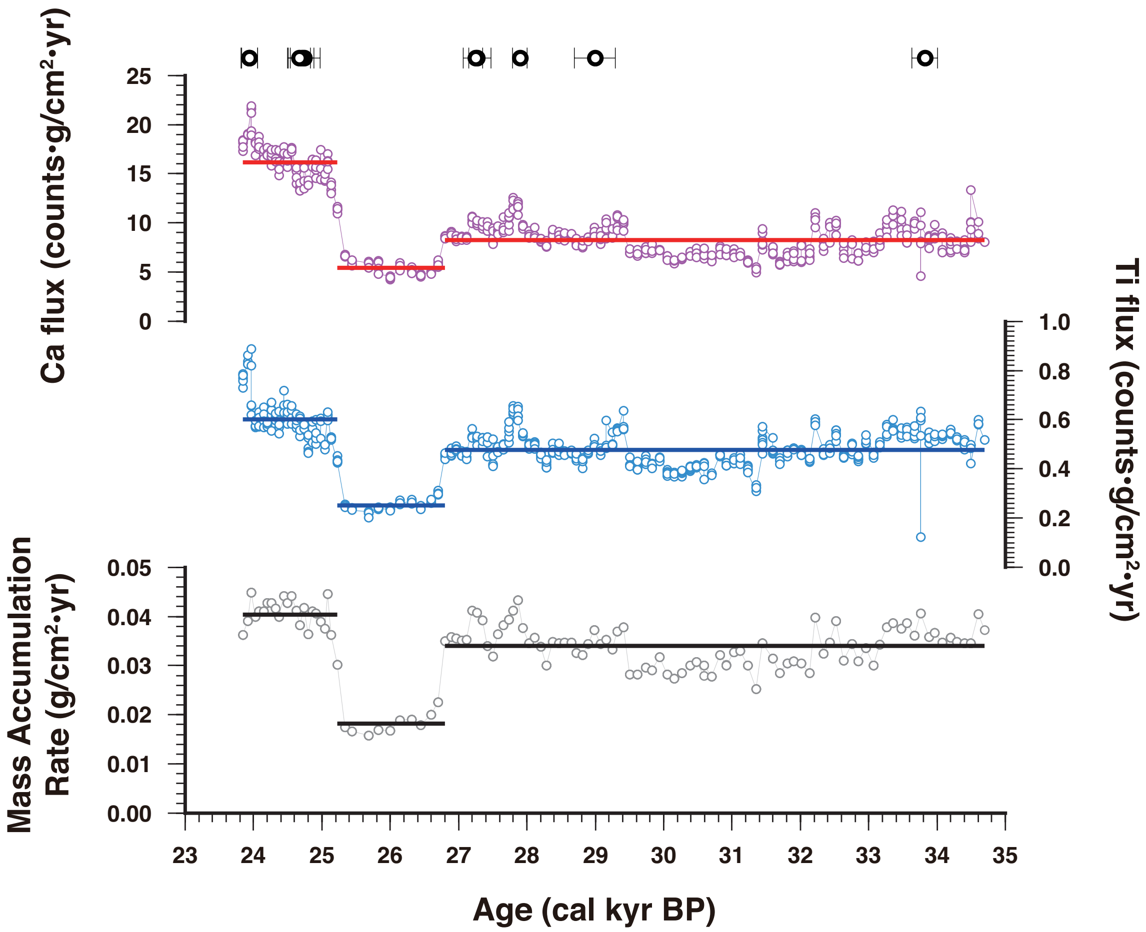

Figure 2.5-2: Ca flux, Ti flux, and mass accumulation rate. Solid lines correspond to the average values during three periods, before ~27 cal kyr BP, during 25–27 cal kyr BP, and after ~25 cal kyr BP. Circles at the top of figure correspond to age control points.

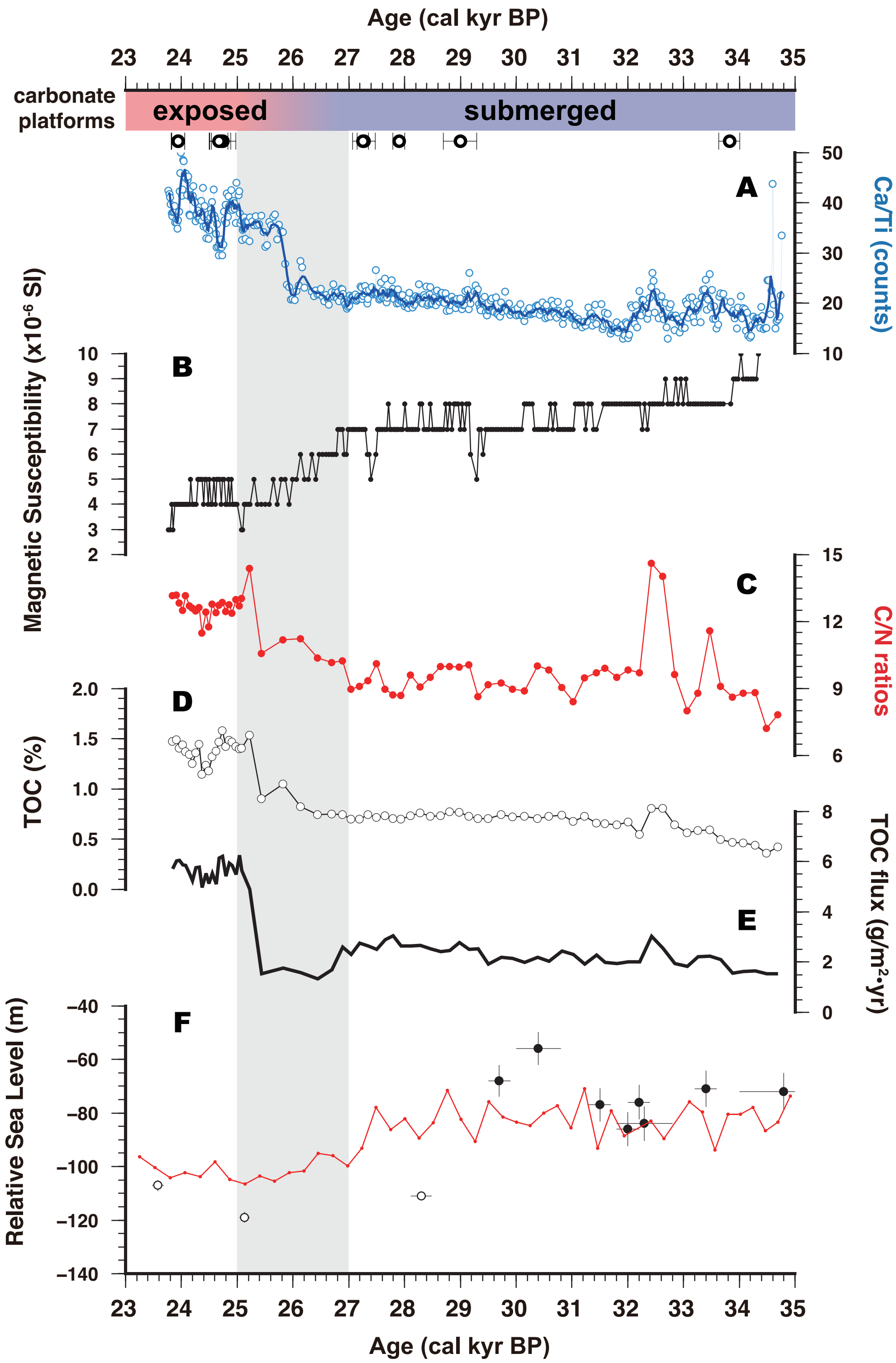

Figure 2.5-3: Ca/Ti ratios, magnetic susceptibility, C/N ratios, TOC, TOC flux, and relative sea-level records. Grey shade corresponds to the timing of carbonate platform exposure due to sea-level fall. A: Ca/Ti ratios. B: Magnetic susceptibility. C: C/N ratios. D: TOC (%). E: TOC flux. F: Relative sea-level records in Huon Peninsula. Black circles correspond to Yokoyama et al. [2001b]. White circles to Cutler et al. [2003]. Red line to Siddall et al. [2003].

2.5.2 Mechanism for sedimentary environmental change

The carbonate terraces and platforms of the outer Bonaparte Gulf are dissected by a network of deeply incised paleochannels that would have been sediment transport pathways during lower sea level (Figure 2.5-4) [Courgeon et al., 2016]. Yokoyama et al. [2000a; 2001a] estimated the age of deposition in these paleochannels to be ca. 17.5 cal kyr BP, suggesting that carbonate sediments were produced and transported to the basin during lower sea level by fluvial activity or ocean currents.

Sedimentation pattern could have fluctuated with the relative strength of monsoon [Gallagher et al., 2014b; Kuhnt et al., 2015]. The Australian Monsoonal precipitation pattern is sensitive to latitudinal ITCZ migration [Lewis et al., 2011], while speleothem records from this region indicate low monsoon variability at ca. 26 cal kyr BP [Lewis et al., 2011; Partin et al., 2007], consistent with marine and terrestrial records [Fitzsimmons et al., 2013; Reeves et al., 2013] that show a northward ITCZ position. I suggest that the changes in monsoonal variability are not strong to control sedimentary facies in the Bonaparte Gulf around 26 cal kyr BP. A relative change in carbonate sediment flux increased at ca. 25 cal kyr BP as shown by physical properties and geochemical analysis (Figure 2.5-3). Rivers pass through the continent would have supplied siliciclastic sediments to the basin [Gingele et al., 2001; Gingele and De Deckker, 2003]. During this period, the supply of siliciclastic sediments did not significantly change due to the weak variability of monsoonal intensity. By contrast, the carbonate supply increased due to exposure of carbonate terraces and platforms.

Sea level below -90 m resulted in sufficient exposure of carbonate terraces and platform to increase the flux of carbonate sediments (Figure 2.5-4). During sea-level highstands, much of the shelf was submerged. During sea-level lowstands, the carbonate terraces and platforms were exposed and the Bonaparte Basin was semi-enclosed from the Timor Sea. The relative area of exposure was an important control on the sedimentary facies of the gulf.

While the hydro-isostatic effects in the Bonaparte Gulf do not affect to the current interpretation [Yokoyama et al., 2000a, 2001a, 2001c], this factor cannot be entirely discounted due to paleotopography and paleo-water depth effects. Yokoyama et al. [2000a, 2001a] estimated the amplitude of this effect (offset between the global sea level and relative sea level) is less than 20 m (see also *Chapter 4*). Therefore, the bathymetry in Figure 2.5-4 has an error of 10% due to hydro-isostasy effects.

These observations indicate that the sedimentary environment in the Bonaparte Gulf is primarily driven by sea-level variability due to the distinctive topography with its central depression surrounded by higher-level carbonate terraces and platforms. Exposure of carbonate terraces and platforms with a sea-level fall enhances sedimentary environmental change, characterized by carbonate sediment production and transportation.

Sea-level change prior into the LGM has been estimated using the uplifted coral on the Huon Peninsula, indicating that sea level fell from -70 to -110 m from 30 to 24 cal kyr BP [Cutler et al., 2003; Yokoyama et al., 2001b]. This is consistent with sea level from the Red Sea [Siddall et al., 2003], which falls ~20 m from 28 to 26 cal kyr BP (-80 to -100 m). This amplitude of a sea-level fall is enough to influence the sedimentary environment in the Bonaparte Gulf.

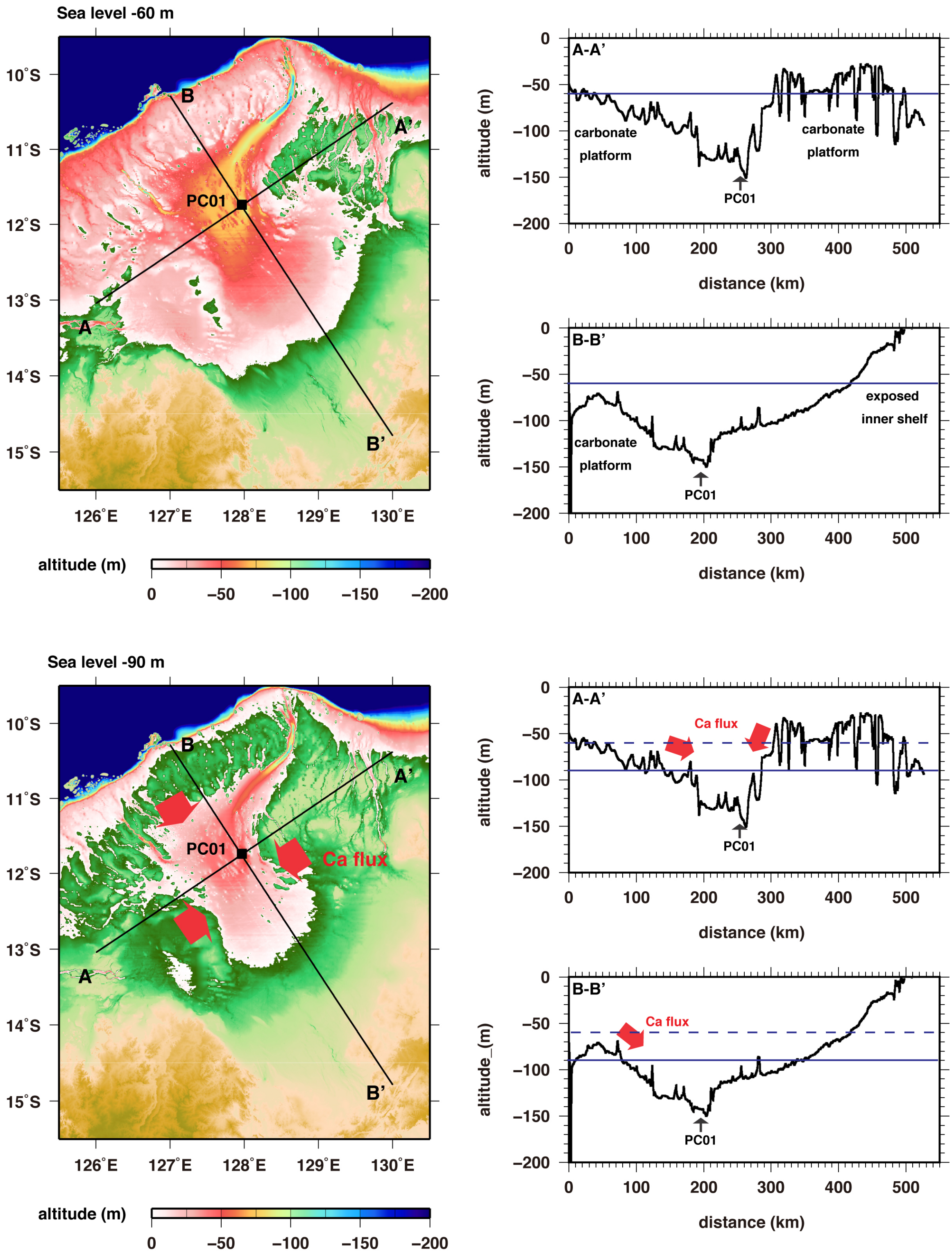

Figure 2.5-4: Bathymetry and sectional views of the Bonaparte Gulf at -60 m and -90 m sea level. Note that there are bathymetric errors estimates in the Bonaparte Gulf due to hydro isostatic effect [Yokoyama et al., 2000a, 2001a]. The effects are relatively minor (see *Chapter 4*).

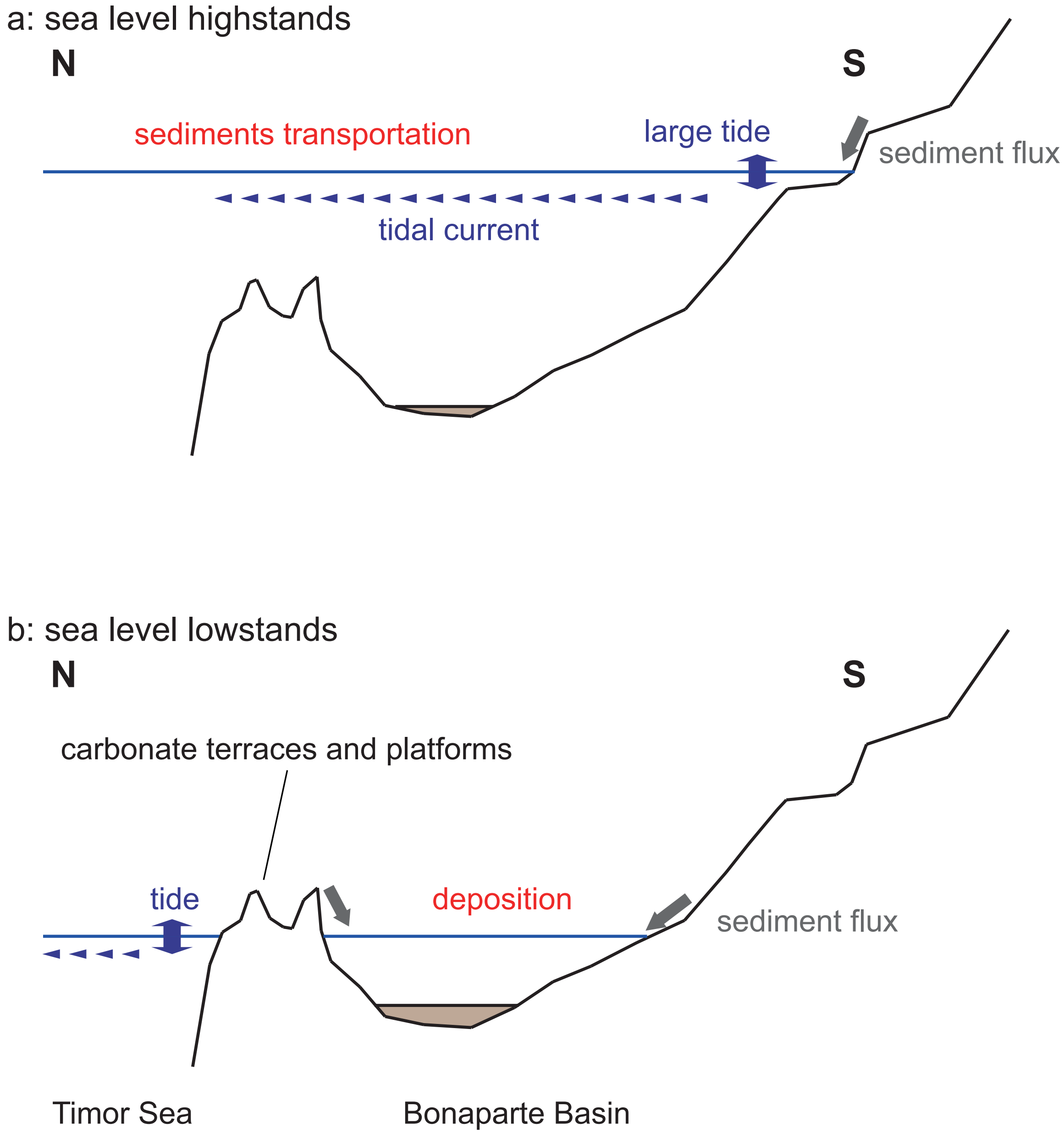

Figure 2.5-6: Schematic transect of the Bonaparte Gulf showing at the period of sea-level highstands (a) and lowstands (b). (a) Sedimentary environments during sea-level highstands. Large tide is observed in inner shelf and sediments transport to the Timor Sea. (b) Sedimentary environments during sea-level lowstands. Deposition in the Bonaparte Basin is enhanced due to exposure of carbonate terraces and platforms.

2.5.3 Comparison to other region

Mixed carbonate-siliciclastic sedimentary systems are observed in low-latitude tropical regions. Isaack et al. [2016] presents a sea-level driven model of sediment dynamics based on a multi-proxy records in the barrier- reef lagoon of Bora Bora in the South Pacific. They suggest that carbonate sediment produced at marginal reef areas and transported to the lagoons. This mechanism indicates that carbonate terraces and platforms in the Bonaparte Gulf can be the source of carbonate sediments, generating the variation of geochemical signal in the core.

The Black Sea becomes a semi-enclosed marginal sea, similar to the Bonaparte Gulf, during lower sea level [Bahr et al., 2005], and reconnected to the Mediterranean Sea at ~ 9,000 years ago associated with sea-level rising [Soulet et al., 2011]. On the basis of geochemical data, the hydrologic system has changed from lacustrine to marine, controlled by a water depth of sills connected to Mediterranean Sea. By contrast, during sea-level lowstands, the Bonaparte Gulf connected to the Timor Sea mainly by paleochannels with the water depth of ~200 m [Yokoyama et al., 2000a, 2001a]. The sedimentary environment in the Bonaparte Gulf is influenced by the exposure of carbonate terraces and platforms, which played a role in pathways of carbonate sediments.

2.6 Summary

Geochemical and chronological records from a piston core in the Bonaparte Gulf, northwestern Australia, show sedimentary environmental change at ca. 26 cal kyr BP. Carbonate terraces and platforms and their deeply incised paleochannels play an important role in this paleoenvironmental change.

Ca/Ti ratios as an indicator of changes in mixed siliciclastic-carbonate sediments increased at ca. 26 cal kyr BP, indicating the enhanced supply of carbonate sediments. TOC and C/N ratios as an indicator of terrestrial input also increased. The changes in these geochemical signals can be explained by the exposure of carbonate terraces and platforms.

Precipitation patterns shift can drive the change in sediment supply. However, during the period I investigate, the variability of Australian monsoon was not strong to change the sedimentary environment. By contrast, global sea-level fall to -90 m occurred at ca. 26 cal kyr BP, driving the exposure of carbonate terraces and platforms and the switch from siliciclastic to carbonate dominated sedimentation. Our research leads the understanding of a sea-level driven sedimentary environmental change in low-latitude mixed siliciclastic-carbonate environment.

Carbonate terraces and platforms in the Bonaparte Gulf protect inner shelf from wave activity of the Timor Sea at lower sea level. Deposition during sea-level lowstands occurs in moderate environments. This indicates that the Bonaparte Gulf is a suitable region to reconstruct sea level change during MIS 2 since there are less possibility of reworking and disturbance.

Chapter 3　Marine Isotope Stage 2 relative sea-level records deduced from sediment cores in the Bonaparte Gulf

本章は，5 年以内に雑誌等で刊行予定のため非公開.

Chapter 4 Ice volume equivalent sea level based on relative sea-level records from the Bonaparte Gulf using glacial isostatic adjustment model

本章は，5 年以内に雑誌等で刊行予定のため非公開．

Chapter 5 General discussion and future perspectives

本章は，5 年以内に雑誌等で刊行予定のため非公開である第 3 章・第 4 章の内容を含むため，一部非公開．

5.1 General discussion

5.1.1 Global sea level change during MIS 2

5.1.2 Implication for mechanism of a sea-level fall to its minimum

5.2 Future perspectives

The new ESL curve demonstrates that the duration of ice volume maximum is ca. 1,000 years during the LGM, suggesting that relative sea level during the LGM would not reach to isostatic equilibrium. This could be a key to solve "missing ice problem" [Lambeck et al., 2000; Clark and Tarasov, 2014].

There are two approaches to constrain ice volume change during the LGM. One is to reconstruct the individual ice sheets using ice model, combined with relative sea level and GPS data in "near-field" regions [cf., Lambeck 1998; Whitehouse et al., 2012; Gowan et al., 2016]. A sum of the individual ice sheets equals to global ice volume. Secondly, far-field relative sea levels provide the information of global ice volume with isostatic corrections [Yokoyama et al., 2000a, 2001a; Lambeck et al., 2014]. The definition of "missing ice problem" is the mismatch between the first and second methods of global ice volume reconstructions [Lambeck et al., 2000; Clark and Tarasov, 2014].

The solution of this problem is required to understand glacial-interglacial climate variability and improve climate modeling to predict future climate change. My ESL curve shows the ca. 1,000 years duration of the LGM, suggesting that each continental ice sheets had experienced the short duration of its maximum, not reaching to isostatic equilibrium. This would derive the overestimation of the maximum volume of each continental ice sheet. This suggestion reduces the offset between a sum of each ice sheet and global ice volume from far-field data. To investigate the validity of this hypothesis, accurate records of each continental ice sheet are required. In addition, uncertainties due to the earth model parameters and potential bias due to today's ice sheet melting should be evaluated precisely in future works.

5.3 Conclusion

List of abbreviation

Abbreviation	Definition
AORI	Atmosphere and Ocean Research Institute
BIIS	British-Irish Ice Sheet
BKIS	Barents-Kara Ice Sheet
cal kyr BP	calendar kilo years before present
CIS	Cordilleran Ice Sheet
cmbsf	cm below sea floor
EAIS	East Antarctic Ice Sheet
ESL	ice volume equivalent sea level
GIA	glacial isostatic adjustment
GIS	Greenland Ice Sheet
IIS	Innuitian Ice Sheet
ITCZ	Intertorpical Convergense Zone
L14	Lambeck et al., 2014
LGM	Last Glacial Maximum
LIS	Laurentide Ice Sheet
MIS	Marine Isotope Stage
psu	practical salinity unit
RSL	relative sea level
SIS	Scandinavian Ice Sheet
TN	total nitrogen
TOC	total organic carbon
WAIS	West Antarctic Ice Sheet
$\delta^{13}C$	stable carbon isotope
H	elastic lithosphere thickness
η_{um}	upper mantle viscosity
η_{lm}	lower mantle viscosity

References

1. Abdul, N.A., Mortlock, R.A., Wright, J.D., Fairbanks, R.G. 2016. Younger Dryas sea level and meltwater pulse 1B recorded in Barbados reef crest coral Acropora palmata. Paleoceanography, 31, 330–344.
2. Abe-Ouchi, A., Saito, F., Kawamura, K., Raymo, M.E., Okuno, J., Takahashi, K., Blatter, H. 2013. Insolation-driven 100,000-year glacial cycles and hysteresis of ice-sheet volume. Nature, 500, 190–193.
3. Adkins, J.F., McIntyre, K., Schrag, D.P. 2002. The salinity, temperature, and $\delta^{18}O$ of the glacial deep ocean. Science, 298, 1769–1773.
4. Anderson, T.J., Nichol, S., Radke, L., Heap, A.D., Battershill, C., Hughes, M., Siwabessy, P.J., Barrie, V., Alvarez de Glasby, B., Tran, M., Daniell, J. 2011. Seabed Environments of the Eastern Joseph Bonaparte Gulf, Northern Australia: GA0325/Sol5117-Post- survey Report. Geoscience Australia Record 2011.08.
5. Argus, D.F., Peltier, W.R., Drummond, R., Moore, A.W. 2014. The Antarctica component of postglacial rebound model ICE-6G_C (VM5a) based on GPS positioning, exposure age dating of ice thicknesses, and relative sea level histories. Geophysical Journal International, 198, 537–563.
6. Athy, L.F. 1930. Density, porosity, and compaction of sedimentary rocks. AAPG Bull, 14, 194–200.
7. Auriac, A., Whitehouse, P.L., Bentley, M.J., Patton, H., Lloyd, J.M., Hubbard, A. 2016. Glacial isostatic adjustment associated with the Barents Sea ice sheet: A modelling inter-comparison. Quaternary Science Reviews, 147, 122–135.
8. Austermann, J., Mitrovica, J.X., Latychev, K., Milne, G.A. 2013. Barbados-based estimate of ice volume at Last Glacial Maximum affected by subducted plate. Nature Geoscience, 6, 553–557.
9. Bahr, A., Lamy, F., Arz, H., Kuhlmann, H., Wefer, G. 2005. Late glacial to Holocene climate and sedimentation history in the NW Black Sea. Marine Geology, 214, 309–322.
10. Bard, E., Hamelin, B., Arnold, M. 1996. Deglacial sea-level record from Tahiti corals and the timing of global meltwater discharge. Nature, 382, 241–244.

11. Bard, E., Hamelin, B., Delanghe-Sabatier, D. 2010. Deglacial meltwater pulse 1B and Younger Dryas sea levels revisited with boreholes at Tahiti. Science, 327, 1235–7.
12. Bard, E., Hamelin, B., Deschamps, P., Camoin, G. 2016. Comment of Younger Drya sea level and meltwater pulse 1B recorded in Barbados reef crest coral Acropora palmata by Abdul et al. (2016 Paleoceanography). Paleoceanography, in press.
13. Bassett, S.E., Milne, G.A., Mitrovica, J.X., Clark, P.U. 2005. Ice sheet and solid earth influences on far-field sea-level histories. Science, 309, 925–928.
14. Berger, A., Loutre, M.F. 1991. Insolation values for the climate of the last 10 million years. Quaternary Science Reviews, 10, 297–317.
15. Blaauw, M., Christen, J.A., 2011. Flexible Paleoclimate Age-Depth Models Using an Autoregressive Gamma Process. Bayesian Analysis, 6, 457–474.
16. Böhm, E., Lippold, J., Gutjahr, M., Frank, M., Blaser, P., Antz, B., Fohlmeister, J., Frank, N., Andersen, M.B., Deininger, M. 2015. Strong and deep Atlantic meridional overturning circulation during the last glacial cycle. Nature, 517, 73–76.
17. Bond, G.C., Heinrich, H., Broecker, W.S., Labeyrie, L., McManus, J. F., Andrews, J. T., Huon, S., Jantschik, R., Clasen, S, Simet, C., Tadesco, K., Klas, M., Bonani, G., Ivy, S. 1992. Evidence for massive discharges of icebergs into the North Atlantic ocean during the last glacial period. Nature, 360, 245–249.
18. Bond, G.C., Showers, W., Elliot, M., Evans, M., Lotti, R., Hajdas, I., Bonani G., Johnson, S. 1999. Mechanisms of Global Climate Change at Millennial Time Scales. Mechanisms of Global Climate Change at Millennial Time Scales. Geophysical Monograph, 112, 35–58.
19. Bourget, J., Ainsworth, R.B., Backé, G., Keep, M. 2012. Tectonic evolution of the northern Bonaparte Basin: impact on continental shelf architecture and sediment distribution during the Pleistocene. Australian Journal of Earth Sciences, 59, 877–897.
20. Bourget. J., Ainsworth, R.B., Nanson, R. 2013. Origin of mixed carbonate and siliciclastic sequences at the margin of a “giant” platform during the Quaternary (Bonaparte Basin, NW Australia). In: Verwer, K., Playton, T.E., Harris, P.M. (Eds.), Deposits, Architecture, and Controls of Carbonate Margin, Slope, and Basinal Settings, Special Publication 105. SEPM (Society for Sedimentary Geology), Tulsa, OK.
21. Bourget, J., Ainsworth, R.B., Thompson, S. 2014. Seismic stratigraphy and

geomorphology of a tide or wave dominated shelf-edge delta (NW Australia): Process-based classification from 3D seismic attributes and implications for the prediction of deep-water sands. Marine and Petroleum Geology, 57, 359–384.

22. Boulton, G.S., Dongelmans, P., Punkari, M., Broadgate, M. 2001. Paleoglaciology of an ice sheet through a glacial cycle: the European ice sheet trough the Weichselian. Quaternary Science Reviews, 20, 591–625.
23. Bowman, G.M. 1985. Oceanic reservoir correction for marine radiocarbon dates from northwestern Australia. Australian Archaeology, 20, 58–67.
24. Carlson, A.E., Clark, P.U. 2012. Ice-Sheet Sources of Sea-Level Rise and Freshwater Discharge During the Last Deglaciation. Reviews of Geophysics, 50, 1–72.
25. Chapman, R.W., Inglis. C. 1902. A.A.A.S. Reports, 9, 67.
26. Chappell, J., Shackleton, N.J. 1986. Oxygen isotopes and sea level. Nature, 324, 137–140.
27. Chappell, J., Ota, Y., Berryman, K. 1996. Late Quaternary coseismic uplift history of Huon Peninsula, Quaternary Science Review 15, 7–22.
28. Chappell, J. 2002. Sea level changes forced ice breakouts in the Last Glacial cycle: New results from coral terraces. Quaternary Science Reviews, 21, 1229–1240.
29. Chivas, A.R., Garc, A., Holt, S., Reeves, J.M., Wheeler, D.J., Switzer, A.D., Murray-Wallance, C.V., Banerjee, D., Price, D.M., Wang, S.X., Pearson, G., Edgar, N.T., Beaufort, L., De Deckker, P., Lawson, E., Cecil, C.B. 2001. Sea-level and environmental changes since the last interglacial in the Gulf of Carpentaria, Australia : an overview, Quaternary International, 85, 19–46.
30. Clark, P.U., Mix, A.C. 2002. Ice sheets and sea level of the Last Glacial Maximum. Quaternary Science Reviews, 21, 1–7.
31. Clark, P.U., McCabe, A.M., Mix, A.C., Weaver, A.J. 2004. Rapid Rise of Sea Level 19,000 Years Ago and Its Global Implications. Science, 304, 1141–1144.
32. Clark, P.U., Dyke, A.S., Shakun, J.D., Carlson, A.E., Clark, J., Wohlfarth, B., Mitrovica, J.X., Hostetler, S.W., McCabe, A.M. 2009. The Last Glacial Maximum. Science, 325, 710–714.
33. Clark, P.U., Tarasov, L. 2014. Closing the sea level budget at the Last Glacial Maximum. Proceedings of the National Academy of Sciences of the United States of America, 111, 15861–15862.

34. Clarke, J.D.A., Bone, Y., Cann, J.H., Davies, M., Macphail, M.K., Wells, F. 2001. Post-glacial from the inner part of Southwest Joseph Bonaparte Gulf. Australian Journal of Earth Sciences, 48, 63–79.
35. Courgeon, S., Bourget, J., Jorry, S.J. 2016. A Pliocene – Quaternary analogue for ancient epeiric carbonate settings : The Malita intrashelf basin (Bonaparte Basin, northwest Australia). AAPG Bulletin, 100, 565–595
36. Cutler, K.B., Edwards, R., Taylor, F.W., Cheng, H., Adkins, J., Gallup, C., Cutler, P. M., Burr, G.S., Bloom, A.L. 2003. Rapid sea-level fall and deep-ocean temperature change since the last interglacial period. Earth and Planetary Science Letters, 206, 253–271.
37. Dalca, A.V., Ferrier, K.L., Mitrovica, J.X., Perron, J.T., Milne, G.A., Creveling, J.R. 2013. On postglacial sea level-III. Incorporating sediment redistribution. Geophysical Journal International, 194, 45–60.
38. Dansgaard, W., White, J.W.C., Johnsen, S.J. 1989. The abrupt termination of the Younger Dryas climate event. Nature, 339, 532–534.
39. De Deckker, P., Yokoyama, Y. 2009. Micropalaeontological evidence for Late Quaternary sea-level changes in Bonaparte Gulf, Australia. Global and Planetary Change, 66, 85–92.
40. De Deckker, P., Barrows, T.T., Rogers, J. 2014. Land-sea correlations in the Australian region: Post-glacial onset of the monsoon in northwestern Western Australia. Quaternary Science Reviews, 105, 181–194.
41. De Deckker, P. 2016. The Indo-Pacific Warm Pool: critical to world oceanography and world climate. Geoscience Letters, 3, 1–12.
42. Deschamps, P., Durand, N., Bard, E., Hamelin, B., Camoin, G., Thomas, A.L., Henderson, G.M., Okuno, J., Yokoyama, Y. 2012. Ice-sheet collapse and sea-level rise at the Bølling warming 14,600 years ago. Nature, 483, 559–564.
43. De Vleeschouwer, F., Pazdur, A., Luthers, C., Streel, M., Mauquoy, D., Wastiaux, C., Le Roux, G., Moschen, R., Blaauw, M., Pawlyta, J., Piotrowska, N. 2012. A millennial record of environmental change in peat deposits from the Misten bog (East Belgium). Quaternary International, 268, 44–57
44. De Vries, H.L., Barendsen, G.W. 1954. Measurements of age by the carbon-14 technique. Nature, 174, 1138–1141.
45. Ding, X., Bassinot, F., Guichard, F., Fang, N.Q. 2013. Indonesian Through flow and monsoon activity records in the Timor Sea since the last glacial maximum. Marine

Micropaleontology, 101, 115–126

46. Divins, D.L. 2003. Total Sediment Thickness of the World's Oceans & Marginal Seas. NOAA National Geophysical Data Center, Boulder, CO.
47. DiNezio, P.N., Clement, A., Vecchi, G.A., Soden, B., Broccoli, A.J., Otto-Bliesner, B.L., Braconnot, P. 2011. The response of the Walker circulation to Last Glacial Maximum forcing: Implications for detection in proxies. Paleoceanography, 26, 1–21.
48. DiNezio, P.N., Tierney, J.E. 2013. The effect of sea level on glacial Indo-Pacific climate. Nature Geoscience, 6, 485–491.
49. DiNezio, P.N., Timmermann, A., Tierney, J.E., Jin, F.F., Otto-Bliesner, B., Rosenbloom, N., Mapes, B., Neale, R., Ivanovic, R.F., Montenegro, A. 2016. The climate response of the Indo-Pacific warm pool to glacial sea level. Paleoceanography, 31, 866–894.
50. Dubois, N., Oppo, D.W., Galy, V.V, Mohtadi, M., van deer Kaars, S., Tierney, J.E., Rosenthal, Y., Eglinton, T.I., Luckage, A., Linsley, B.K. 2014. Indonesian vegetation response to changes in rainfall seasonality over the past 25, 000 years, Nature Geoscience, 7, 513–517.
51. Dutton, A., Carlson, A.E., Long, A.J., Milne, G.A., Clark, P.U., DeConto, R., Horton, B.P., Rahmstorf, M., Raymo, M.E. 2015. Sea-level rise due to polar ice-sheet mass loss during past warm periods. Science, 349, aaa4019-1–9.
52. Dyke, A.S., Andrews, J.T., Clark, P.U., England, J.H., Miller, G.H., Shaw, J., Veillette, J.J. 2002. The Laurentide and Innuitian ice sheets during the Last Glacial Maximum. Quaternary Science Reviews, 21, 9–31.
53. Dziewonski, A.M., Anderson, D.L. 1981. Preliminary reference Earth model. Physics of the Earth and Planetary Interiors, 25, 297–356
54. Edwards, R.L., Beck, J.W., Burr, G.S., Donahue, D.J., Chappell, J.M.A., Bloom, A. L., Druffel, E.R.M., Taylor, F.W. 1993. A Large Drop in Atmospheric $^{14}C/^{12}C$ and Reduced Melting in the Younger Dryas, Documented with ^{230}Th Ages of Corals. Science, 260, 962–968.
55. Egbert, G.D., Erofeeva, S.Y. 2002. Efficient inverse modeling of barotropic ocean tides. Journal of Atmospheric and Oceanic Technology, 19, 183–204.
56. Egbert, G.D., Ray, R.D., Bills, B.G. 2004. Numerical modeling of the global semidiurnal tide in the present day and in the last glacial maximum. Journal of Geophysical Research, 109, 1–15.

57. Esat, T.M., Mcculloch, M.T., Chappell, J., Pillans, B., Omura, A. 1999. Rapid Fluctuations in Sea Level Recorded at Huon Peninsula During the Penultimate Deglaciation. Science, 283, 197–201.
58. Emiliani, C. 1955. Pleistocene temperatures. The Journal of Geology, 63, 538–578.
59. Fairbanks R.G. 1989. A 17,000-year glacio-eustatic sea level record: influence of glacial melting rates on the Younger Dryas event and deep-ocean circulation. Nature, 342, 637–642.
60. Farrell, W.E., Clark, J.A. 1976. On Postglacial Sea Level. Geophysical Journal of the Royal Astronomical Society, 46, 647–667.
61. Fenton, M., Geiselhart, S., Rohling, E.J., Hemleben, C. 2000. Aplanktonic zones in the Red Sea. Marine Micropaleontology, 40, 277–294.
62. Fitzsimmons, K.E., Cohen, T.J., Hesse, P.P., Jansen, J., Nanson, G.C., May, J., Barrows, T.T., Haberlah, D., Hilger, A., Kell, T., Larsen, J., Lomax. J., Treble, P. 2013. Late Quaternary palaeoenvironmental change in the Australian drylands. Quaternary Science Reviews, 74, 78–96.
63. Fleming, K., Johnston, P., Zwartz, D., Yokoyama, Y., Lambeck, K., Chappell, J. 1998. Refining the eustatic sea level curve since the Last Glacial Maximum using far and intermediate field sites. Earth and Planetary Science Letters, 163, 327–342.
64. Fleming, K., Lambeck, K. 2004. Constraints on the Greenland Ice Sheet since the Last Glacial Maximum from sea-level observations and glacial-rebound models. Quaternary Science Reviews, 23, 1053–1077.
65. Gallagher, S.J., Fulthorpe, C.S., Bogus, K.A. 2014a. Reefs, oceans, and climate: a 5 million year history of the Indonesian Throughflow, Australian monsoon, and subsidence on the northwest shelf of Australia. International Ocean Discovery Program Scientific Prospectus 356
66. Gallagher, S.J., Wallace, M.W., Hoiles, P.W., Southwood, J.M. 2014b. Seismic and stratigraphic evidence for reef expansion and onset of aridity on the Northwest Shelf of Australia during the Pleistocene. Marine and Petroleum Geology, 57, 470–481.
67. Gingele, F.X., De Deckker, P., Hillenbrand, C.D. 2001. Clay mineral distribution in surface sediments between Indonesia and NW Australia-source and transport by ocean currents. Marine Geology, 179, 135–146.
68. Gingele, F.X., De Deckker, P. 2003. Fingerprinting Australia's Rivers Using Clays and the Application for the Marine Record of Rapid Climate Change. Advances in Regolith: 140–143

69. Gowan, E.J., Tregoning, P., Purcell, A., Montillet, J.P., McClusky, S. 2016. A model of the western Laurentide Ice Sheet, using observations of glacial isostatic adjustment. Quaternary Science Reviews, 139, 1–16.
70. Grant, K.M., Rohling, E.J., Bar-Matthews, M., Ayalon, A., Medina-Elizalde, M., Ramsey, C.B., Satow, C., Roberts, A.P. 2012. Rapid coupling between ice volume and polar temperature over the past 150,000 years. Nature, 491, 744–747.
71. Grant, K.M., Rohling, E.J., Ramsey, C.B., Cheng, H., Edwards, R.L., Florindo, F., Heslop, D., Marra, F., Roberts, A.P., Tamisiea, M.E., Williams, F. 2014. Sea-level variability over five glacial cycles. Nature Communications, 5, 5076.
72. Griffiths, S.D., Peltier, W.R. 2009. Modeling of polar ocean tides at the Last Glacial Maximum: Amplification sensitivity, and climatological implications. Journal of Climate, 22, 2905–2924.
73. Guillocheau, F., Rouby, D., Robin, C., Helm, C., Rolland, N., Le Carlier de Veslud, C., Braun, J. 2012. Quantification and causes of the terrigeneous sediment budget at the scale of a continental margin: A new method applied to the Namibia-South Africa margin. Basin Research, 24, 3–30.
74. Haig, D.W. 2012. Palaeobathymetric gradients across Timor during 5.7-3.3Ma (latest Miocene-Pliocene) and implications for collision uplift. Palaeogeography, Palaeoclimatology, Palaeoecology, 331–332, 50–59.
75. Hanebuth, T., Stattegger, K., Grootes, P.M. 2000. Rapid Flooding of the Sunda Shelf: A Late-Glacial Sea-Level Record. Science, 288, 1033–1035.
76. Hanebuth, T., Stattegger, K., Bojanowski, A. 2009. Termination of the Last Glacial Maximum sea-level lowstand: The Sunda-Shelf data revisited. Global and Planetary Change, 66, 76–84.
77. Hanebuth, T.J.J., Voris, H.K., Yokoyama, Y., Saito, Y., Okuno, J. 2011. Formation and fate of sedimentary depocentres on Southeast Asia's Sunda Shelf over the past sea-level cycle and biogeographic implications. Earth-Science Reviews, 104, 92–110.
78. Heinrich, H. 1988. Origin and consequences of cyclic ice rafting in the Northeast Atlantic Ocean during the past 130,000 years. Quaternary Research, 29, 142–152.
79. Hemleben, C., Meischner, D., Zahn, R., Almogi-Labin, A., Erlenkeuser, H., Hiller, B. 1996. Three hundred eighty thousand year long stable isotope and faunal records from the Red Sea: Influence of global sea level change on hydrography. Paleoceanography, 11, 147–156.

80. Hemming, S.R. 2004. Heinrich events: Massive late Pleistocene ditritus layers of the North Atlanitc and their global cliamate imprint. Reviews of Geophysics, 42, 1–43.
81. Hibbert, F.D., Rohling, E.J., Dutton, A., Williams, F.H., Chutcharavan, P.M., Zhao, C., Tamisiea, M.E. 2016. Coral indicators of past sea-level change : A global repository of U-series dated benchmarks. Quaternary Science Reviews, 145, 1–56.
82. Horton, B.P., Edwards, R.J. 2006. Quantifying Holocene sea level change using intertidal foraminifera: lessons from the British Isles. Cushman Foundation for Foraminiferal Research, Special Publication vol. 40. 97pp.
83. Hughes, P.D., Gibbard, P.L. 2015. A stratigraphical basis for the Last Glacial Maximum (LGM). Quaternary International, 383, 174–185.
84. Isaack, A., Gischler, E., Hudson, J.H., Anselmetti, F.S., Lohner, A., Vogel, H., Garbode, E., Camoin, G.F. 2016 A new model evaluating Holocene sediment dynamics : Insights from a mixed carbonate – siliciclastic lagoon (Bora Bora, Society Islands, French Polynesia, South Pacific). Sedimentary Geology, 343, 99–118.
85. Ishiwa, T., Yokoyama, Y., Miyairi, Y., Ikehara, M., Obrochta, S. 2016a. Sedimentary environmental change induced from late Quaternary sea-level change in the Bonaparte Gulf, northwestern Australia. Geoscience Letters, 3, 1–11.
86. Ishiwa, T., Yokoyama, Y., Miyairi, Y., Obrochta, S., Sasaki, T., Kitamura, A., Suzuki, K., Ikehara, M., Ikehara, K., Kimoto, K., Bourget, J., Matsuzaki, H. 2016b. Reappraisal of sea-level lowstand during the Last Glacial Maximum observed in the Bonaparte Gulf sediments, northwestern Australia. Quaternary International, 397, 373–379.
87. Ivins, E.R., James, T.S. 2005. Antarctic glacial isostatic adjustment: a new assessment. Antarctic Science, 17, 541–553.
88. Johnston, P., Lambeck, K. 1999. Postglacial rebound and sea level contributions to changes in the geoid and the Earth's rotation axis. Geophysical Journal International, 136, 537–558.
89. Jull, A.J.T., Burr, G.S., Hodgins, G.W.L. 2013. Radiocarbon dating, reservoir effects, and calibration. Quaternary International, 299, 64–71.
90. Kido, Y., Koshikawa, T., Tada, R. 2006. Rapid and quantitative major element analysis method for wet fine-grained sediments using an XRF microscanner. Marine Geology, 229, 209–225.
91. Kuhnt, W., Holbourn, A., Xu, J., Opdyke, B., De Deckker, P., Mudelsee, M. 2015.

Southern Hemisphere control on Australian monsoon variability during the late deglaciation and Holocene. Nature Communications, 6, 5916.

92. Kusch, S., Eglinton, T.I., Mix, A.C., Mollenhauer, G. 2010. Timescales of lateral sediment transport in the Panama Basin as revealed by radiocarbon ages of alkenones, total organic carbon and foraminifera. Earth and Planetary Science Letters, 290, 340–350.
93. Lamb, A.L., Wilson, G.P., Leng, M.J. 2006. A review of coastal palaeoclimate and relative sea-level reconstructions using δ13C and C/N ratios in organic material. Earth-Science Reviews, 75, 29–57.
94. Lambeck, K., Nakada, M. 1990. Late Pleistocene and Holocene sea-level change along the Australian coast. Palaeogeography, Palaeoclimatology, Palaeoecology, 89, 143–176.
95. Lambeck, K., Nakada, M. 1992. Constraints on the age and duration of the last interglacial period and on sea-level variations. Nature, 357, 125–128.
96. Lambeck K. 1993. Glacial Rebound of the British Isles II: A high resolution, high-precision model. Geophysical Journal International, 115, 960–990.
97. Lambeck, K. 1995. Constraints on the Late Weichselian ice sheet over the Barents Sea from observations of raised shorlines. Quaternary Science Reviews, 14, 1-16
98. Lambeck, K., Smither, C., Johnston, P. 1998. Sea-level change, glacial rebound and mantle viscosity for northern Europe. Geophysical Journal International, 134, 102–144.
99. Lambeck, K., Yokoyama, Y., Johnston, P., Purcell, A. 2000. Global ice volumes at the Last Glacial Maximum and early Lateglacial. Earth and Planetary Science Letters, 181, 513–527.
100. Lambeck, K., Chappell, J. 2001. Sea Level Change Through the Last Glacial Cycle. Science, 679, 679–687.
101. Lambeck, K. 2002. Sea level change from mid Holocene to Recent time: An Australian example with global implications. Ice Sheets, Sea Level and the Dynamic Earth, 29, 33–50.
102. Lambeck, K., Esat, T.M., Potter, E.K. 2002a. Links between climate and sea levels for the past three million years. Nature, 419, 199–206.
103. Lambeck, K., Yokoyama, Y., Purcell, T. 2002b. Into and out of the Last Glacial Maximum: sea-level change during Oxygen Isotope Stages 3 and 2. Quaternary Science Reviews, 21, 343–360.

104. Lambeck, K., Purcell, A., Johnston, P., Nakada, M., Yokoyama, Y. 2003. Water-load definition in the glacio-hydro-isostatic sea-level equation. Quaternary Science Reviews, 22, 309–318.
105. Lambeck, K., Purcell, A. 2003. Glacial rebound & crustal stress in Finland. Technical Report 2003-10, Posiva Oy, Olkiluoto, Finland.
106. Lambeck, K., Purcell, A., Zhao, J., Svensson, N.O. 2010. The scandinavian ice sheet: From MIS 4 to the end of the last glacial maximum. Boreas, 39, 410–435.
107. Lambeck, K., Rouby, H., Purcell, A., Sun, Y., Sambridge, M. 2014. Sea level and global ice volumes from the Last Glacial Maximum to the Holocene. Proceedings of the National Academy of Sciences, 111, 15296–303.
108. Lamprell, K., Whitehead, T. 1992. Molluscs of Australia Volume1. Bathurst, N.S.W: Crawford House Press
109. Lamprell, K., Healy, J. 1998. Molluscs of Australia Volume2. Bathurst, N.S.W: Crawford House Press.
110. Lavering, I.H. 1993. Quaternary and modern environments of the Van Diemen Rise, Timor Sea, and potential effects of additional petroleum exploration activity. AGSO Journal of Australian Geology and Geophysics., 13, 281–292.
111. Lees, B.G. 1992a. Recent terrigenous sedimentation in Joseph Bonaparte Gulf, Northwestern Australia. Marine geology, 103, 199–213.
112. Lees, B.G. 1992b. The development of a chenier sequence on the Victoria Delta, Joseph Bonaparte Gulf, northern Australia. Marine Geology, 103, 215–224.
113. Lewis, S.C., Gagan, M.K., Ayliffe, L.K., Zhao, J., Hantoro, W.S., Treble, P.C., Hellstrom, J.C., LeGrande, A.N., Kelley, M., Schmidt, G.A., Suwargadi, B.W. 2011. High-resolution stalagmite reconstructions of Australian – Indonesian monsoon rainfall variability during Heinrich stadial 3 and Greenland interstadial 4. Earth and Planetary Science Letters, 303, 133–142.
114. Li, C., Chen, Q., Zhang, J., Yang, S., Fan, D. 2000. Stratigraphy and paleoenvironmental changes in the Yangtze Delta during the Late Quaternary. Journal of Asian Earth Sciences, 18, 453–469.
115. Lisiecki, L.E., Raymo, M.E. 2005. A Pliocene-Pleistocene stack of 57 globally distributed benthic $\delta^{18}O$ records. Paleoceanography, 20, 1–17.
116. Liu, J., Milne, G.A., Kopp, R.E., Clark, P.U., Shennan, I. 2015. Sea-level constraints on the amplitude and source distribution of Meltwater Pulse 1A. Nature Geoscience, 9, 6–12.

117. Longley, I.M., Buessenschuett, C., Clydsdale, L., Cubitt, C.J., Davis, R.C., Johnson, M.K., Marshall, N.M., Murray, A.P., Somerville, R., Spry, T.B., Thompson, N.B. 2002. The North West Shelf of Australia–a Woodside perspective. The sedimentary basins of Western Australia, 3, 27–88.
118. Louis, J.P., Radok, J.R.M. 1975. Propagation of Tidal Waves in the Joseph Bonaparte Gulf. Journal of Geophysical Research, 80, 1689–1670.
119. Mackie, E.A.V., Leng, M.J., Lloyd, J.M., Arrowsmith, C. 2005. Bulk organic δ13C and C/N ratios as palaeosalinity indicators within a Scottish isolation basin. Journal of Quaternary Science, 20, 303–312.
120. Mackie, E.A.V, Lloyd, J.M., Leng, M.J., Bentley, M.J., Arrowsmith, C. 2007. Assessment of $\delta^{13}C$ and C/N ratios in bulk organic matter as palaeosalinity indicators in Holocene and Lateglacial isolation basin sediments, northwest Scotland. Journal of Quaternary Science, 22, 579–591.
121. Manabe, S., Broccoli, A.J. 1985. The influence of continental ice sheets on the climate of an ice age. Journal of Geophysical Research, 90, 2167–2190.
122. Milne, G.A., Mitrovica, J.X. 1996. Postglacial sea-level change on a rotating Earth. Geophysical Journal International, 126, F13–F20.
123. Mitrovica, J.X., Forte, A.M. 2004. A new inference of mantle viscosity based upon joint inversion of convection and glacial isostatic adjustment data. Earth and Planetary Science Letters, 225, 177–189.
124. Mix, A.C., Bard, E., Schneider, R. 2001. Environmental processes of the ice age: land, ocean, glaciers (EPILOG). Quaternary Science Reviews, 20, 627–657.
125. Mohtadi, M., Oppo, D.W., Steinke, S., Stuut, J.W., Pol-holz, R. De, Hebbeln, D., Lückge, A. 2011. Glacial to Holocene swings of the Australian – Indonesian monsoon. Nature Geoscience, 4, 540–544.
126. Mortlock, R.A., Adbul, N.A., Wright, J.D., Fairbanks, R.G. 2016. Younger Dryas sea level slow stand and meltwater pulse 1B recorded in Barbados reef crest Acropora palmata reply to a comment Bard et al. (2016) in press, paleoceanography, 31.
127. Naafs, B.D.A., Hefter, J., Stein, R. 2013a. Millennial-scale ice rafting events and Hudson Strait Heinrich(-like) Events during the late Pliocene and Pleistocene: A review. Quaternary Science Reviews, 80, 1–28.

128. Naafs, B.D.A., Hefter, J., Grützner, J., Stein, R. 2013b. Warming of surface waters in the mid-latitude North Atlantic during Heinrich events. Paleoceanography, 28, 153–163.
129. Nakada, M., Lambeck, K. 1987. Glacial rebound and relative sea-level variations: a new appraisal. Geophysical Journal of the Royal Astronomical Society, 90, 171–224.
130. Nakada, M., Okuno, J. 2003. Perturbations of the Earth's rotation and their implications for the present-day mass balance of both polar ice caps. Geophysical Journal International, 152, 124–138.
131. Nakada, M., Karato, S.I. 2012. Low viscosity of the bottom of the Earth's mantle inferred from the analysis of Chandler wobble and tidal deformation. Physics of the Earth and Planetary Interiors, 192, 68-80.
132. Nakada, M., Okuno, J., Yokoyama, Y. 2016. Total meltwater volume since the Last Glacial Maximum and viscosity structure of Earth's mantle inferred from relative sea level changes at Barbados and Bonaparte Gulf and GIA-induced J2. Geophysical Journal International, 204, 1237–1253.
133. Nakada, M., Okuno, J. 2016. Inference of mantle viscosity for depth resolutions of GIA observations. Geophysical Journal International, 207, 719–740.
134. Nakamura, A., Yokoyama, Y., Maemoku, H., Yagi, H., Okamura, M., Matsuoka, H., Miyake, N., Osada, T., Teramura, H., Adhikari, D.P., Dangol, V., Miyairi, Y., Obrochta, S., Matsuzaki, H. 2012. Late Holocene Asian monsoon variations recorded in Lake Rara sediment, western Nepal. Journal of Quaternary Science, 27, 125–128.
135. Nakamura, A., Yokoyama, Y., Maemoku, H., Yagi, H., Okamura, M., Matsuoka, H., Miyake, N., Osada, T., Adhikari P.D., Dangol, V., Ikehara, M., Miyairi, Y., Matsuzaki, H. 2016. Weak monsoon event at 4.2 ka recorded in sediment from Lake Rara, Himalayas. Quaternary International, 397, 349–359
136. Nicholas, W.A., Nichol, S.L., Howard, F.J.F, Picard, K., Dulfer, H., Radke, L.C., Carroll, A.G., Tran, M., Siwabessy, P.J.W. 2014. Pockmark development in the Petrel Sub-basin, Timor Sea, Northern Australia : Seabed habitat mapping in support of CO2 storage assessments. Continental Shelf Research, 83, 129–142.
137. North Greenland Ice Core Project members. 2004. High-resolution record of Northern Hemisphere climate extending into the last interglacial period. Nature, 431, 147–151.

138. Obrochta, S.P., Miyahara, H., Yokoyama, Y., Crowley, T.J. 2012. A re-examination of evidence for the North Atlantic "1500-year cycle" at Site 609. Quaternary Science Reviews, 55, 23–33.
139. Obrochta, S.P., Yokoyama, Y., Morén, J., Crowley, T.J. 2014. Conversion of GISP2-based sediment core age models to the GICC05 extended chronology. Quaternary Geochronology, 20, 1–7.
140. O'Connor, S., Ulm, S., Fallon, S.J., Barham, A., Loch, I. 2010. Pre-bomb marine reservoir variability in the Kimberley Region, Western Australia. Radiocarbon, 52, 1158–1165.
141. Ohkouchi, N., Eglinton, T.I., Keigwin, L.D., Hayes, J.M. 2002. Spatial and temporal offsets between proxy records in a sediment drift. Science, 298, 1224–1227.
142. Oka, A., Hasumi, H., Abe-Ouchi, A. 2012. The thermal threshold of the Atlantic meridional overturning circulation and its control by wind stress forcing during glacial climate. Geophysical Research Letters, 39, 1–6.
143. Okutani, T. 2000. Marine Mollusks in Japan. University of Tokyo Press, 1173 pp.
144. Otto-Bliesner, B.L., Brady, E.C. 2010. The sensitivity of the climate response to the magnitude and location of freshwater forcing: last glacial maximum experiments. Quaternary Science Reviews, 29, 56–73.
145. Partin, J.W., Cobb, K.M., Adkins, J.F., Clark, B., Fernandez, D.P. 2007. Millennial-scale trends in west Pacific warm pool hydrology since the Last Glacial Maximum. Nature, 449, 452–455
146. Peltier, W.R. 2004. Global glacial isostasy and the surface on the ice-age earth: the ICE-5G (VM2) Model and GRACE. Annual Review Earth Planetary Science, 32,111–149
147. Peltier, W.R., Fairbanks, R.G. 2006. Global glacial ice volume and Last Glacial Maximum duration from an extended Barbados sea level record. Quaternary Science Reviews, 25, 3322–3337.
148. Peltier, W.R., Argus, D.F., Drummond, R. 2015. Space geodesy constrains ice age terminal deglaciation: The global ICE-6G-C (VM5a) model. Journal of Geophysical Research B: Solid Earth, 120, 450–487.
149. Pico, T., Mitrovica, J.X., Ferrier, K.L., Braun, J. 2016. Global ice volume during MIS 3 inferred from a sea-level analysis of sedimentary core records in the Yellow River Delta. Quaternary Science Reviews, 152, 72–79.

150. Przeslawski, R., Alvarez, B., Battershill, C., Smith, T. 2014. Sponge biodiversity and ecology of the Van Diemen Rise and eastern Joseph Bonaparte Gulf, northern Australia. Hydrobiologia, 730, 1–16.
151. Ramsey, C.B., Lee, S. 2013. Recent and planned developments of the program Oxcal. Radiocarbon, 55, 720–730.
152. Raymond, P.A, Bauer, J.E. 2001. Riverine export of aged terrestrial organic matter to the North Atlantic Ocean. Nature, 409, 497–500.
153. Reeves, J.M., Bostock, H.C., Ayliffe, L.K., Barrows, T.T., De Deckker, P., Devriendt, L.S., Dunbar, G.B., Drysdale, R.N., Fitzsimmons, K.E., Gagan, M.K., Griffiths, M.L., Haberle, S.G., Jansen, J.D., Krause, C., Lewis, S., McGregor, H,V., Mooney, S.D., Moss, P., Nanson, G.C., Purcell, A., van der Kaars, S. 2013. Palaeoenvironmental change in tropical Australasia over the last 30,000 years – a synthesis by the OZ-INTIMATE group. Quaternary Science Reviews, 74, 97–114
154. Reimer, P.J., Bard, E., Bayliss, A., Beck, J.W., Blackwell, P.G., Ramsey, C.B., Buck, C.E., Cheng, H., Edwards, R.L., Friedrich, M., Grootes, P.M., Guilderson, T.P., Haflidason, H., Hajdas, I., Hatte, C., Heaton, T.J., Hoffmann, D.L., Hogg, A.G., Hughen, K.A., Kaiser, K.F., Kromer, B., Manning, S.W., Niu. M., Reimer, R.W., Richards, D.A., Scott, E.M., Southon, J.R., Staff, R.A., Turney, C.S.M., van der Plicht, J. 2013. Intcal13 and marine13 radiocarbon age calibration curves 0 –50,000 years cal bp. Radiocarbon, 55, 1869–1887
155. Riethdorf, J.R., Thibodeau, B., Ikehara, M., Nurnberg, D., Max, L., Tiedemann, R., Yokoyama, Y. 2015. Surface nitrate utilization in the Bering sea since 180kA BP: Insight from sedimentary nitrogen isotopes. Deep-Sea Research Part II: Topical Studies in Oceanography, 1–14.
156. Rohling, E.J., Foster, G.L., Grant, K.M., Marino, G., Roberts, A.P., Tamisiea, M.E., Williams, F. 2014. Sea-level and deep-sea-temperature variability over the past 5.3 million years. Nature, 508, 477–82.
157. Ruddiman, W.F., McIntyre, A., Niebler-Hunt, V., Durazzi, J.T. 1980. Oceanic evidence for the mechanism of rapid northern hemisphere glaciation. Quaternary Research, 13, 33–64.
158. Sakamoto, T., Kuroki, K., Sugawara, T., Aoike, K., Iijima, K., Sugisaki, S. 2006. Non-Destructive X-Ray Fluorescence (XRF) Core-Imaging Scanner, TATSCAN-F2, Scientific Drilling, 2, 37–39.

159. Sclater, J.G., Christie, P.A.F. 1980. Continental stretching: An explanation of the Post-Mid-Cretaceous subsidence of the central North Sea Basin. Journal of Geophysical Research: Solid Earth, 85, 3711–3739.
160. Shackleton, N.J. 1967. Oxygen Isotope Analyses and Pleistocene Temperatures Re-assessed. Nature, 215, 15–17.
161. Shackleton, N.J. 1987. Oxygen isotopes, ice volume and sea level. Quaternary Science Reviews, 6, 183–190.
162. Shakun, J.D., Carlson, A.E. 2010. A global perspective on Last Glacial Maximum to Holocene climate change. Quaternary Science Reviews, 29, 1801–1816.
163. Shanahan, T.M., Beck, J.W., Overpeck, J.T., McKay, N.P., Pigati, J.S., Peck, J.A., Scholz, C.A., Heil, C.W., King, J. 2012. Late Quaternary sedimentological and climate changes at Lake Bosumtwi Ghana: New constraints from laminae analysis and radiocarbon age modeling. Palaeogeography, Palaeoclimatology, Palaeoecology, 361-362, 49–60.
164. Shennan, I., Milne, G. 2003. Sea-level observations around the Last Glacial Maximum from the Bonaparte Gulf, NW Australia. Quaternary Science Reviews, 22, 1543–1547.
165. Shennan, I., Long, A.J., Horton, B.P. 2015. Handbook of sea-level research. American Geophysical Union, 600pp.
166. Siddall, M., Rohling, E., Almogi-Labin, A., Hemleben, C., Meischner, D., Schmelzer, I., Smeed, D.A. 2003. Sea-level fluctuations during the last glacial cycle. Nature, 423, 853–858.
167. Simon, K.M., James, T.S., Henton, J.A., Dyke, A.S. 2016. A glacial isostatic adjustment model for the central and northern Laurentide Ice Sheet based on relative sea level and GPS measurements, Geophysical Journal International, 205, 1618–1636.
168. Soulet, G., Ménot, G., Lericolais, G., Bard, E. 2011. A revised calendar age for the last reconnection of the Black Sea to the global ocean. Quaternary Science Review, 30, 1019–1026.
169. Steffen, H., Kaufmann, G. 2005. Glacial isostatic adjustment of Scandinavia and northwestern Europe and the radial viscosity structure of the Earth's mantle. Geophysical Journal International, 163, 801–812.
170. Toyofuku, T., Suzuki, M., Suga, H., Sakai, S., Suzuki, A., Ishikawa, T., de Nooijer, L.J., Schiebel, R., Kawahata, H., Kitazato, H. 2011. Mg/Ca and $\delta^{18}O$ in the brackish

shallow-water benthic foraminifer Ammonia “beccarii.” Marine Micropaleontology, 78, 113–120.

171. Uehara, K., Saito, Y. 2003. Late Quaternary evolution of the Yellow/East China Sea tidal regime and its impacts on sediments dispersal and seafloor morphology. Sedimentary Geology, 162, 25–38.
172. Uehara, K., Scourse, J.D., Horsburgh, K.J., Lambeck, K., Purcell, A.P. 2006. Tidal evolution of the northwest European shelf seas from the Last Glacial Maximum to the present. Journal of Geophysical Research: Oceans, 111, 1–15.
173. Uehara, K., 2012. Estimating Bottom Stress on Continental Shelves from Tidal and Wave Models. Reports of Research Institute fro Applied Mechanics, Kyushu University, 143, 69–73.
174. van Andel, T., Heath, G., Moore, T., McGeary, D.F. 1967. Late Quaternary History, Climate, and Oceanography of the Timor Sea northwestern Australia. American Journal of Science, 265, 737–758.
175. Vettoretti, G., Peltier, W.R. 2013. Last Glacial Maximum ice sheet impacts on North Atlantic climate variability: The importance of the sea ice lid. Geophysical Research Letters, 40, 6378–6383.
176. Waelbroeck, C., Labeyrie, L., Michel, E., Duplessy, J.C., McManus, J.F., Lambeck, K., Balbon, E., Labracherie, M. 2002. Sea-level and deep water temperature changes derived from benthic foraminifera isotopic records. Quaternary Science Reviews, 21, 295–305.
177. Ward, S.L., Neill, S.P., Scourse, J.D., Bradley, S.L., Uehara, K. 2016. Sensitivity of palaeotidal models of the northwest European shelf seas to Glacial Isostatic Adjustment since the Last Glacial Maximum. Quaternary Science Reviews, 151, 198–211.
178. Whitehouse, P.L., Bentley, M.J., Le Brocq, A.M. 2012. A deglacial model for Antarctica: Geological constraints and glaciological modelling as a basis for a new model of Antarctic glacial isostatic adjustment. Quaternary Science Reviews, 32, 1–24.
179. Whiteway, T. 2009. Australian Bathymetry and Topography Grid, June 2009. Scale 1:5000000. Geoscience Australia, Canberra.
180. Wiedicke, M., Kudrass, H.R., Hübscher, C. 1999. Oolitic beach barriers of the last Glacial sea-level lowstand at the outer Bengal shelf. Marine Geology, 157, 7–18.

181. Yassini, I., Jones, B.G. 1995. Recent Foraminifera and Ostracoda from Estuarine and Shelf Environments on the South-eastern Coast of Australia. University of Wollongong Press, Wollongong. 484 pp.
182. Yokoyama, Y., Lambeck, K., De Deckker, P., Johnston, P., Fifield, L.K. 2000a. Timing of the Last Glacial Maximum from observed sea-level minima. Nature, 406, 713–716.
183. Yokoyama, Y., Esat, T.M., Lambeck, K., Fifield, L.K. 2000b. Last ice age millennial scale climate changes recorded in Huon Peninsula corals. Radiocarbon, 42, 383–401.
184. Yokoyama, Y., De Deckker, P., Lambeck, K., Johnston, P., Fifield, L.K. 2001a. Sea-level at the Last Glacial Maximum: evidence from northwestern Australia to constrain ice volumes for oxygen isotope stage 2. Palaeogeography, Palaeoclimatology, Palaeoecology, 165, 281–297.
185. Yokoyama, Y., Esat, T.M., Lambeck, K. 2001b. Coupled climate and sea-level changes deduced from Huon Peninsula coral terraces of the last ice age. Earth and Planetary Science Letters, 193, 579–587
186. Yokoyama, Y., Purcell, A., Lambeck, K., Johnston, P. 2001c. Shore-line reconstruction around Australia during the Last Glacial Maximum and Late Glacial Stage. Quaternary International, 83–85, 9–18.
187. Yokoyama, Y., De Deckker, P., Lambeck, K. 2003. Reply to "Sea-level observations around the Last Glacial Maximum from the Bonaparte Gulf, NW Australia" by I. Shennan and G. Milne. Quaternary Science Reviews, 22, 1549–1550.
188. Yokoyama, Y., Purcell, A., Marshall, J.F., Lambeck, K. 2006. Sea-level during the early deglaciation period in the Great Barrier Reef, Australia. Global and Planetary Change, 53, 147–153.
189. Yokoyama, Y., Miyairi, Y., Matsuzaki, H., Tsunomori, F. 2007. Relation between acid dissolution time in the vacuum test tube and time required for graphitization for AMS target preparation. Nuclear Instruments and Methods in Physics, 259, 330–334
190. Yokoyama, Y., Esat, T.M. 2011. Global climate and sea level: Enduring variability and rapid fluctuations over the past 150,000 years. Oceanography, 24, 54–69
191. Yokoyama, Y., Maeda, Y., Okuno, J., Miyairi, Y., Kosuge, T. 2016a. Holocene Antarctic melting and lithospheric uplift history of the southern Okinawa trough inferred from mid- to late-Holocene sea level in Iriomote Island, Ryukyu, Japan. Quaternary International, 397, 342–348.

192. Yokoyama, Y., Anderson, J.B., Yamane, M., Simkins, L.M., Miyairi, Y., Yamazaki, T., Koizumi, M., Suga, H., Kusahara, K., Prothro, L., Hasumi, H., Southon, J.R., Ohkouchi, N. 2016b. Widespread collapse of the Ross Ice Shelf during the late Holocene. Proceedings of the National Academy of Sciences, 113, 2354–2359
193. Yu, F., Zong, Y., Lloyd, J.M., Huang, G., Leng, M.J., Kendrick, C., Lamb, A.L., Yim, W.W.S. 2010. Bulk organic $\delta^{13}C$ and C/N as indicators for sediment sources in the Pearl River delta and estuary, southern China. Estuarine, Coastal and Shelf Science, 87, 618–630.
194. Zhang, X., Lohmann, G., Knorr, G., Purcell, C. 2014. Abrupt glacial climate shifts controlled by ice sheet changes. Nature, 512, 290–294.